

Relativistic Shocks: Particle Acceleration and Magnetization

L. Sironi · U. Keshet · M. Lemoine

Received: date / Accepted: date

Abstract We review the physics of relativistic shocks, which are often invoked as the sources of non-thermal particles in pulsar wind nebulae (PWNe), gamma-ray bursts (GRBs), and active galactic nuclei (AGN) jets, and as possible sources of ultra-high energy cosmic-rays. We focus on particle acceleration and magnetic field generation, and describe the recent progress in the field driven by theory advances and by the rapid development of particle-in-cell (PIC) simulations. In weakly magnetized or quasi parallel-shocks (*i.e.* where the magnetic field is nearly aligned with the flow), particle acceleration is efficient. The accelerated particles stream ahead of the shock, where they generate strong magnetic waves which in turn scatter the particles back and forth across the shock, mediating their acceleration. In contrast, in strongly magnetized quasi-perpendicular shocks, the efficiencies of both particle acceleration and magnetic field generation are suppressed. Particle acceleration, when efficient, modifies the turbulence around the shock on a long time scale, and the accelerated particles have a characteristic energy spectral index of $s_\gamma \simeq 2.2$ in the ultra-relativistic limit. We discuss how this novel understanding of particle acceleration and magnetic field generation in relativistic shocks can be applied to high-energy astrophysical phenomena, with an emphasis on PWNe and GRB afterglows.

All authors contributed equally to this review.

L. Sironi
Harvard-Smithsonian Center for Astrophysics, Cambridge, MA, 02138, USA
E-mail: lsironi@cfa.harvard.edu

U. Keshet
Physics Department, Ben-Gurion University of the Negev, Be'er-Sheva 84105, Israel
E-mail: ukeshet@bgu.ac.il

M. Lemoine
Institut d'Astrophysique de Paris, CNRS - UPMC, 98 bis boulevard Arago, F-75014 Paris, France
E-mail: lemoine@iap.fr

Keywords acceleration of particles · galaxies: active · gamma rays: bursts · magnetic fields · pulsars: general · radiation mechanisms: non-thermal · relativistic processes

1 Introduction

In pulsar wind nebulae (PWNe), gamma-ray bursts (GRBs), and jets from active galactic nuclei (AGNs), signatures of non-thermal processes are revealed by power-law radiation spectra spanning an extremely wide range of wavelengths, from radio to X-rays, and beyond. Yet, it is still a mystery how the emitting particles can be accelerated up to ultra-relativistic energies and how the strong magnetic fields are generated, as required in order to explain the observations. In most models, non-thermal particles and near-equipartition fields are thought to be produced at relativistic shock fronts, but the details of the mechanisms of particle acceleration and magnetic field generation are still not well understood.

Particle acceleration in shocks is usually attributed to the Fermi process, where particles are energized by bouncing back and forth across the shock. Despite its importance, the Fermi process is still not understood from first principles. The highly nonlinear coupling between accelerated particles and magnetic turbulence – which is generated by the particles, and at the same time governs their acceleration – is extremely hard to incorporate in analytic models. Only in recent years, thanks to major breakthroughs on analytical and numerical grounds, has our understanding of the Fermi process in relativistic shocks significantly advanced. This is the subject of the present review.

Relativistic shocks pose some unique challenges with respect to their non-relativistic counterparts. For example, the distribution of accelerated particles can no longer be approximated as isotropic if the shock is relativistic. In a relativistic shock, the electric and magnetic fields significantly mix as one switches between upstream and downstream frames of reference. And unlike non-relativistic shocks, where some aspects of the theory can be tested by direct spacecraft measurements, relativistic shocks are only constrained by remote observations. For recent reviews of relativistic shocks, see [Bykov and Treumann \(2011\)](#); [Bykov et al. \(2012\)](#).

This chapter is organized as follows. First, we review recent analytical advances on the theory of particle acceleration in relativistic shocks, arguing that the accelerated particle spectrum and its power-law slope in the ultra-relativistic limit, $s_\gamma \equiv -d \log N / d \log \gamma \simeq 2.2$ (where γ is the particle Lorentz factor), are fairly robust (Section 2). Here, we assume *a priori* that some magnetic turbulence exists on both sides of the shock, such that the Fermi process can operate. Next, we describe the plasma instabilities that are most relevant for generating this turbulence (Section 3), stressing the parameter regime where the so-called Weibel (or “filamentation”) instability – which is often thought to mediate the Fermi process in weakly magnetized relativistic shocks – can grow. Then, we summarize recent findings from particle-in-cell

(PIC) simulations of relativistic shocks, where the non-linear coupling between particles and magnetic waves can be captured from first principles (Section 4). Finally, we describe the astrophysical implications of these results for the acceleration of ultra high energy cosmic rays (UHECRs) and for the radiative signatures of PWNe and GRB afterglows (Section 5; for a review of PWNe, see Kargaltsev et al. (2015) in the present volume; for a review of GRBs, see Racusin et al. (2015) in the present volume). We briefly conclude in Section 6.

2 Particle Acceleration in Relativistic Shocks

Diffusive (Fermi) acceleration of charged particles in collisionless shocks is believed to be responsible for the production of non-thermal distributions of energetic particles in many astronomical systems (Blandford and Eichler 1987; Malkov and Drury 2001, but see, *e.g.* Arons and Tavani (1994) for a discussion of alternative shock acceleration processes). The Fermi acceleration process in shocks is still not understood from first principles: particle scattering in collisionless shocks is due to electromagnetic waves formed around the shock, but no present analytical formalism self-consistently calculates the generation of these waves, the scattering and acceleration of particles, and the backreaction of these particles on the waves and on the shock itself.

The theory of particle acceleration was first developed mainly by evolving the particle distribution under some Ansatz for the scattering mechanism (*e.g.* diffusion in pitch angle), within the “test particle” approximation, where modifications of wave and shock properties due to the high energy particles are neglected. This phenomenological approach proved successful in explaining the spectrum of relativistic particle distributions inferred from observations, although a more careful approach is needed to account for the energy fraction deposited in each particle species (electrons, positrons, protons, and possibly heavier ions), and to test the Ansatz of the scattering prescription.

For *non-relativistic* shocks, the linear theory of diffusive particle acceleration, first developed in 1977 (Krymskii 1977; Axford et al. 1978; Bell 1978; Blandford and Ostriker 1978), yields a power-law distribution $d^3N/d^3p \propto p^{-s_p}$ of particle momenta p , with a spectral index

$$s_p = s_\gamma + 2 = 3\beta_u/(\beta_u - \beta_d). \quad (1)$$

Here, β is the fluid velocity normalized to the speed of light c in the frame of the shock, which is assumed planar and infinite, and subscripts u (d) denote the upstream (downstream) plasma. For strong shocks in an ideal gas of adiabatic index $\Gamma = 5/3$, this implies $s_p = 4$ (*i.e.* $s_\gamma = 2$; constant energy per logarithmic energy interval, since $p^2 d^3N/d^3p \propto p^{-2}$), in agreement with observations.

The lack of a characteristic momentum scale, under the above assumptions, implies that the spectrum remains a power-law in the relativistic case, as verified numerically (Bednarz and Ostrowski 1998; Achterberg et al. 2001). The particle drift downstream of the shock implies that more particles are moving downstream than upstream; this anisotropy is of order of β_u when

measured in the downstream frame (Keshet and Waxman 2005). Thus, while particle anisotropy is negligible for non-relativistic shocks, the distribution becomes highly anisotropic in the relativistic case, even when measured in the more isotropic downstream frame. Consequently, one must simultaneously determine the spectrum and the angular distribution of the particles, which is the main difficulty underlying the analysis of test particle acceleration when the shock is relativistic.

Observations of GRB afterglows led to the conclusion that highly relativistic collisionless shocks produce a power-law distribution of high energy particles with $s_p = 4.2 \pm 0.2$ (Waxman 1997; Freedman and Waxman 2001; Berger et al. 2003). This triggered a numerical investigation of particle acceleration in such shocks, showing that s_p indeed approaches the value of 4.2 for large shock Lorentz factors ($\gamma_u \equiv (1 - \beta_u^2)^{-1/2} \gg 1$), in agreement with GRB observations, provided that particle scattering is sufficiently isotropic.

The spectral index s_p was calculated under the test particle approximation for a wide range of shock velocities, various equations of state, and different scattering prescriptions. This was achieved by approximately matching numerical eigenfunctions of the transport equation between upstream and downstream (Kirk and Schneider 1987; Heavens and Drury 1988; Kirk et al. 2000), by Monte Carlo simulations (Bednarz and Ostrowski 1998; Achterberg et al. 2001; Ellison and Double 2002; Lemoine and Pelletier 2003; Niemiec and Ostrowski 2004; Lemoine and Revenu 2006; Ellison et al. 2013), by expanding the distribution parallel to the shock front (Keshet and Waxman 2005), and by solving for moments of the angular distribution (Keshet 2006).

These studies have assumed rest frame diffusion in pitch angle or in the angle between particle velocity and shock normal. These two assumptions yield similar spectra in the limit of ultra-relativistic shocks (Ostrowski and Bednarz 2002). As discussed later in this review, one expects these assumptions to hold at relativistic shocks. However, some scenarios involve the conversion of the accelerated species into a neutral state and then back – *e.g.* proton to neutron and then back to proton via photo-hadronic interactions (Derishev et al. 2003) or electron to photon and then back to electron through Compton and pair production interactions (Stern and Poutanen 2008) – in which case the particle may have time to suffer a large angle deflection upstream of the shock, leading to large energy gains and generically hard spectra (Bednarz and Ostrowski 1998; Meli and Quenby 2003; Blasi and Vietri 2005).

For isotropic, small-angle scattering in the fluid frame, expanding the particle distribution about the shock grazing angle (Keshet and Waxman 2005) leads to a generalization of the non-relativistic Eq. (1) that reads

$$s_p = (3\beta_u - 2\beta_u\beta_d^2 + \beta_d^3)/(\beta_u - \beta_d), \quad (2)$$

in agreement with numerical studies (Kirk et al. 2000; Achterberg et al. 2001) over the entire range of β_u and β_d . In particular, in the ultra-relativistic shock limit, the spectral index becomes

$$s_p(\beta_u \rightarrow 1, \beta_d \rightarrow 1/3) = 38/9 = 4.222\dots \quad (3)$$

The spectrum is shown in Fig. 1 for different equations of state, as a function of the shock four-velocity $\gamma_u\beta_u$.

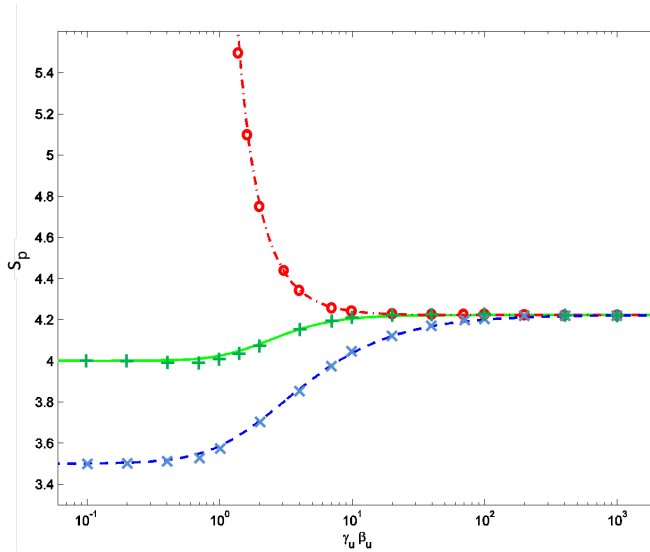


Fig. 1 Spectral index according to Eq. (2) (Keshet and Waxman 2005, curves) and to a numerical eigenfunction method (Kirk et al. 2000, symbols), as a function of $\gamma_u\beta_u$, for three different types of shocks (Kirk and Duffy 1999): a strong shock with the Jüttner/Synge equation of state (solid curve and crosses), a strong shock with fixed adiabatic index $\Gamma = 4/3$ (dashed curve and x-marks), and for a relativistic gas where $\beta_u\beta_d = 1/3$ (dash-dotted curve and circles).

The above analyses assumed that the waves scattering the particles move, on average, with the bulk fluid velocity. More accurately, one should replace β by the mean velocity of the waves that are scattering the particles. In the shock precursor (see §3.1), the scattering waves are expected to be slower than the incoming flow, leading to a softer spectrum (smaller β_u in Eq. 2).

Small-angle scattering can be parameterized by the angular diffusion function $\mathcal{D} \equiv \langle (\Delta\theta)^2 / \Delta t \rangle$, where θ is the angle of the particle velocity, taken here with respect to the shock normal, and angular brackets denote an ensemble average. The function $\mathcal{D} = \mathcal{D}(\theta, p, z)$ should be specified on both sides of the shock, and in general depends on θ , on the particle momentum p , and on its distance z from the shock front.

For scattering off waves with a small coherence length $\lambda \ll r_L$, where $r_L = (pc/eB)$ is the Larmor radius, roughly $(r_L/\lambda)^2$ uncorrelated scattering events are needed in order to produce an appreciable deflection, so $\mathcal{D} \sim r_L^2 c / \lambda \propto p^2$ (Achterberg et al. 2001; Pelletier et al. 2009). Here, B is the magnetic field, and e is the electron's charge. Simulations (Sironi et al. 2013) confirm this scaling at early times; some implications are discussed in Section 4. The precise dependence of \mathcal{D} upon z is not well known. It is thought that

\mathcal{D} slowly and monotonically declines away from the shock, as the energy in self-generated fields decreases. However, the extents of the upstream precursor and downstream magnetized region are not well constrained observationally, and in general are numerically inaccessible in the foreseeable future.

For an evolved magnetic configuration, it is natural to assume that the diffusion function is approximately separable in the form $\mathcal{D} = D(\theta)D_2(p, z)$. Here, D_2 (which may be approximately separable as well, but see [Katz et al. 2007](#)) can be eliminated from the transport equation by rescaling z , such that the spectrum depends only on the angular part $D(\theta)$.

The spectrum is typically more sensitive to the downstream diffusion function D_d than it is to the upstream D_u . In general, an enhanced D_d along (opposite to) the flow yields a softer (harder) spectrum; the trend is roughly reversed for D_u ([Keshet 2006](#)). Thus, the spectrum may deviate significantly from that of isotropic diffusion, in particular in the ultra-relativistic limit ([Kirk et al. 2000](#); [Keshet 2006](#)). However, the spectral slope s is not sensitive to localized changes in D at angles perpendicular to the flow ([Keshet 2006](#)). For roughly forward-backward symmetric scattering in the downstream frame, as suggested by PIC simulations, s is approximately given by its isotropic diffusion value in Eq. 2 ([Keshet et al.](#), in preparation).

Particle acceleration is thought to be efficient, at least in weakly magnetized or quasi-parallel shocks, as discussed below. Thus, the relativistic particles are expected not only to generate waves, but also to slow down and heat the bulk plasma ([Blandford and Eichler 1987](#)). As particles with higher energies are expected to diffuse farther upstream and slow the plasma, lower-energy particles are effectively accelerated by a slower upstream. Consequently, if the scattering waves are assumed to move with the bulk plasma, the spectrum would no longer be a power-law. However, this effect may be significant only for mildly relativistic shocks, with Lorentz factors below $\gamma_u \sim 3$ ([Ellison and Double 2002](#); [Ellison et al. 2013](#)).

To understand the energy, composition, and additional features of the accelerated particles, such as the acceleration time and energy cutoffs, one must not only analyze the scattering of these particles (for example, by deriving \mathcal{D}), but also address the injection problem, namely the process by which a small fraction of particles becomes subject to significant acceleration. Such effects were investigated using Monte-Carlo techniques ([Bednarz and Ostrowski 1998](#); [Ellison et al. 2013](#)), in the so-called “thermal leakage” model, where fast particles belonging to the downstream Maxwellian are assumed to be able to cross the shock into the upstream. More self-consistent results on particle injection based on PIC simulations are presented in Section 4. To uncover the physics behind the injection and acceleration processes, we next review the generation of electromagnetic waves in relativistic shocks.

3 Plasma Instabilities in Relativistic Shocks

3.1 The Shock Precursor

The collisionless shock transition is associated with the build-up of some electromagnetic barrier, which is able to slow down and nearly isotropize the incoming unshocked plasma. In media of substantial magnetization¹, $\sigma \gtrsim 10^{-2}$, this barrier can result from the compression of the background magnetic field (as a result of the Lorentz transformation to the frame of a relativistic shock, the most generic configuration is that of a quasi-perpendicular field), while at lower magnetizations, it is understood to arise from the generation of intense micro-turbulence in the shock “precursor”, as explained hereafter and illustrated in Fig. 2.

At high magnetization, the gyration of the ambient particles in the background compressed magnetic field can trigger a synchrotron maser instability, which sends precursor electromagnetic waves into the upstream (Langdon et al. 1988; Hoshino and Arons 1991; Hoshino et al. 1992; Gallant et al. 1992). As incoming electrons and positrons interact with these waves, they undergo heating (Hoshino 2008; Sironi and Spitkovsky 2011b), but acceleration seemingly remains inefficient (Section 4.1).

At magnetizations $\sigma \lesssim 10^{-2}$, the interpenetration of the incoming background plasma and the supra-thermal particles, which have been reflected on the shock front or which are undergoing Fermi cycles around the shock, leads to anisotropic micro-instabilities over an extended region in front of the shock, called the “precursor” here. These instabilities then build up a magnetic barrier, up to a level² $\epsilon_B \sim 10^{-2} - 10^{-1}$, sufficient to deflect strongly the incoming particles and thus mediate the shock transition. This picture, first envisioned by Moiseev and Sagdeev (1963), has been recently demonstrated in *ab initio* PIC simulations (Spitkovsky 2005; Kato 2007; Spitkovsky 2008a). The generation of micro-turbulence in the shock precursor is thus a key ingredient in the formation of the shock and in the development of the Fermi process, as anticipated analytically (Lemoine et al. 2006) and from Monte Carlo simulations (Niemić et al. 2006), and demonstrated by PIC simulations (Spitkovsky 2008b; Sironi and Spitkovsky 2009a, 2011b), see hereafter.

As seen in the background plasma (upstream) rest frame, the supra-thermal particles form a highly focused beam, with an opening angle $\sim 1/\gamma_u$ and a mean Lorentz factor $\bar{\gamma}_{|u} \sim \gamma_u^2$. In contrast, boosting back to the shock frame, this supra-thermal particle distribution is now open over $\sim \pi/2$, with a mean

¹ The magnetization is defined as $\sigma = B^2 / [4\pi\gamma_u(\gamma_u - 1)n'mc^2]$ in terms of B , the large-scale background magnetic field measured in the shock front rest frame, and n' , the proper upstream particle density. The mass m is m_p for an electron-proton shock, and m_e for an electron-positron shock, *i.e.* it corresponds to the mass of the particles which carry the bulk of the inertia. For a perpendicular shock, in which the background magnetic field in the shock frame is perpendicular to the flow, the magnetization can also be written as $\sigma = (u_A/c)^2$, with u_A the Alfvén four-velocity of the upstream plasma.

² The parameter ϵ_B denotes the magnetization of the turbulence, $\epsilon_B = \delta B^2 / [4\pi\gamma_u(\gamma_u - 1)n'mc^2]$, where δB is the fluctuating magnetic field.

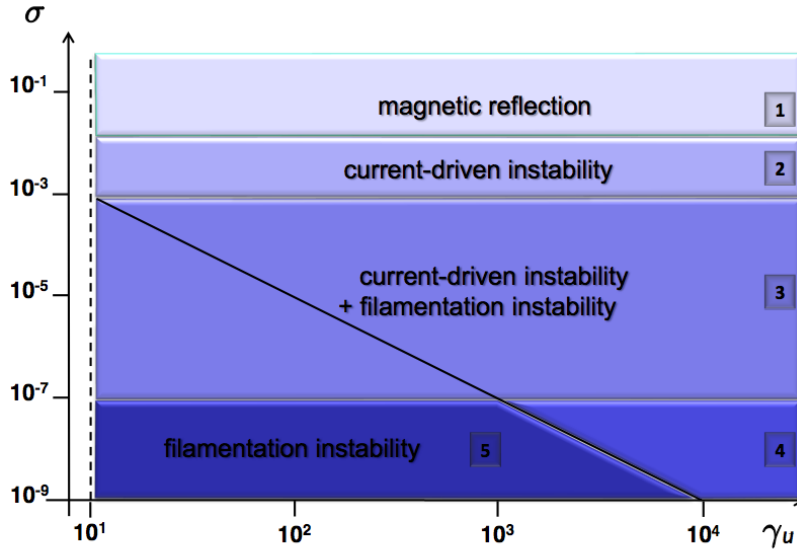


Fig. 2 Phase diagram of relativistic collisionless shocks in the plane (γ_u, σ) ; this figure assumes $\gamma_u > 10$ and $\xi_{\text{cr}} = 0.1$, where the parameter $\xi_{\text{cr}} = e_{\text{cr}} / [\gamma_u(\gamma_u - 1)n' mc^2]$ characterizes the energy density of supra-thermal particles (e_{cr}) relative to the incoming energy flux, as measured in the shock rest frame. In region 1, the shock transition is initiated by magnetic reflection in the compressed background field, while in regions 2 – 5, the magnetic barrier is associated to the growth of micro-instabilities, as indicated. The solid diagonal line indicates values of σ and γ_u above which the filamentation instability would not have time to grow, in the absence of deceleration resulting from the compensation of the perpendicular current of the supra-thermal particles gyrating in the background field. See Section 3.1 and Lemoine et al. (2014a) for a detailed discussion.

Lorentz factor $\bar{\gamma}_{\text{sh}} \gtrsim \gamma_u$, while the incoming plasma is highly focused, with a mean Lorentz factor γ_u . A host of micro-instabilities can in principle develop in such anisotropic configurations, see the general discussion by Bret (2009). However, in the deep relativistic regime, the restricted length scale of the precursor imposes a strong selection of potential instabilities, since a background plasma volume element remains subject to the growth of instabilities only while it crosses the precursor. In the shock rest frame, this time scale is $t_{\times, B} \simeq \omega_c^{-1}$ in the presence of a quasi-perpendicular background field³ (a common field geometry in relativistic flows), or $t_{\times, \delta B} \simeq \gamma_u \epsilon_B^{-1} \omega_p^{-1} (\omega_p \lambda_{\delta B} / c)^{-1}$ if the scattering is dominated by short scale turbulence of magnetization ϵ_B and coherence length $\lambda_{\delta B}$ (assuming that the waves are purely magnetic in the rest frame of the background plasma), see *e.g.* Milosavljević and Nakar

³ $\omega_c \equiv eB_{|u}/mc$ represents the upstream frame cyclotron frequency (and $B_{|u}$ is the magnetic field in the upstream frame) while $\omega_p \equiv (4\pi n' e^2/m)^{1/2}$ denotes the plasma frequency.

(2006a), Lemoine and Pelletier (2010) and Plotnikov et al. (2013). This small length scale implies that only the fastest modes can grow, which limits the discussion to a few salient instabilities.

Before proceeding further, one should stress that the above estimates for t_{\times} do not account for the influence of particles accelerated to higher energies, which can propagate farther into the upstream plasma and thus seed instabilities with smaller growth rate and on larger spatial scales. While such particles do not carry the bulk of the energy if the spectral index $s_{\gamma} > 2$, it is anticipated that they should nevertheless influence the structure of the precursor, see in particular Milosavljević and Nakar (2006a), Katz et al. (2007), Medvedev and Zakutnyaya (2009), Pelletier et al. (2009) and Reville and Bell (2014) for general analytical discussions, as well as Keshet et al. (2009) for an explicit numerical demonstration of their potential influence. Similarly, the above estimates do not make a distinction between electron-positron and electron-ion shocks; in particular, it is understood that ω_c and ω_p refer to the species which carries the bulk of the energy (*i.e.* ions for electron-ion shocks). PIC simulations have demonstrated that in electron-ion shocks, electrons are heated in the precursor to nearly equipartition with the ions, meaning that in the shock transition their relativistic inertia becomes comparable to that of ions (*e.g.* Sironi et al. 2013); hence one does not expect a strong difference between the physics of electron-positron and electron-ion shocks from the point of view of micro-instabilities, and unless otherwise noted, this difference will be omitted in the following. The microphysics of electron heating in the precursor nevertheless remains an important open question, see Gedalin et al. (2008), Gedalin et al. (2012), Plotnikov et al. (2013) and Kumar et al. (2015) for recent discussions of this issue; indeed, the average Lorentz factor of electrons at the shock transition directly impacts the peak frequency of the synchrotron radiation of relativistic blast waves.

In the context of relativistic weakly magnetized shocks, the most celebrated instability is the Weibel-like filamentation mode, which develops through a charge separation in the background plasma, triggered by magnetic fluctuations which segregate particles of opposite charges into current filaments of alternate polarity (*e.g.* Gruzinov and Waxman 1999; Medvedev and Loeb 1999; Wiersma and Achterberg 2004; Lyubarsky and Eichler 2006; Achterberg and Wiersma 2007; Achterberg et al. 2007; Lemoine and Pelletier 2010; Bret et al. 2010; Rabinak et al. 2011; Lemoine and Pelletier 2011; Nakar et al. 2011; Shaisultanov et al. 2012). The current carried by the particles then positively feeds the magnetic fluctuations, leading to fast growth, even in the absence of a net large-scale magnetic field. In the rest frame of the background plasma, this instability grows in the linear regime as fast as⁴ $\Im\omega \simeq \xi_{\text{cr}}^{1/2}\omega_p$, with maximum growth on scales of the order of c/ω_p ; in the filament rest frame, this instability is mostly of magnetic nature, *i.e.* $\Re\omega \sim 0$. Several branches of this instability have been discussed in the literature, in particular the “oblique mode”, which

⁴ The maximal growth rate of the Weibel instability is related to the plasma frequency of the beam of supra-thermal particles, ω_{pb} , though $\Im\omega \simeq \omega_{\text{pb}}$, with $\omega_{\text{pb}} \simeq \xi_{\text{cr}}^{1/2}\omega_p$.

involves a resonance with electrostatic modes. Even though this latter mode grows slightly faster than the fully transverse filamentation mode, it suffers from Landau damping once the electrons are heated to relativistic temperatures, while the transverse filamentation mode appears relatively insensitive to temperature effects. Thus, at a first order approximation, the transverse filamentation mode indeed appears to dominate the precursor at very low magnetizations. Its non-linear evolution, however, remains an open question; analytical estimates suggest that it should saturate at values $\epsilon_B \ll 10^{-2}$ via trapping of the particles (Wiersma and Achterberg 2004; Lyubarsky and Eichler 2006; Achterberg and Wiersma 2007; Achterberg et al. 2007), while PIC simulations see a continuous growth of magnetic energy density even when the non-linear filamentary structures have been formed (*e.g.* Keshet et al. 2009; Sironi et al. 2013). Whether additional instabilities such as a kinking of the filaments contribute in the non-linear phase thus remains debated, see for instance Milosavljević and Nakar (2006b).

At moderate magnetization levels, another fast instability can be triggered by the perpendicular current (transverse to both the magnetic field and the shock normal) seeded in the precursor by the supra-thermal particles during their gyration around the background field (Lemoine et al. 2014a,b). The compensation of this current by the background plasma on its entry into the precursor leads to a deceleration of the flow, which modifies somewhat the effective timescale available for the growth of plasma instabilities, and destabilizes the modes of the background plasma. The growth rate for this instability can be as large as $\Im\omega \sim \omega_p$, indicating that it can compete with the Weibel filamentation mode at moderate magnetizations. If the supra-thermal particle beam carries a net charge (in the shock rest frame), or a net transverse current, other similar instabilities are to be expected (*e.g.* Pelletier et al. 2009; Casse et al. 2013; Reville and Bell 2014). The phase space study of Lemoine et al. (2014a) concludes that the filamentation mode likely dominates at magnetization levels $\sigma \lesssim 10^{-7}$, while this perpendicular current-driven instability dominates at $10^{-3} \lesssim \sigma \lesssim 10^{-2}$; in between, both instabilities combine to form a complex precursor structure. Interestingly, these results do not seem to depend on the shock Lorentz factor, in good agreement with PIC simulations (Sironi and Spitkovsky 2009a, 2011b; Sironi et al. 2013).

Finally, one should mention the particular case of quasi-parallel (subluminal) configurations: there, a fraction of the particles can in principle escape to infinity along the magnetic field and seed other, larger scale, instabilities. One prime candidate is the relativistic generalization of the Bell streaming instability (*e.g.* Milosavljević and Nakar 2006a; Reville et al. 2006), which is triggered by a net longitudinal current of supra-thermal particles; this instability has indeed been observed in PIC simulations (Sironi and Spitkovsky 2011b). Of course, such a parallel configuration remains a special case in the deep relativistic regime. In mildly relativistic shock waves, with $\gamma_u \beta_u \sim 1$, locally parallel configurations become more frequent, hence one could expect such instabilities to play a key role in seeding large scale turbulence.

3.2 Downstream Magnetized Turbulence

How the magnetized turbulence evolves downstream of the shock is an important question, with direct connections to observations. The previous discussion suggests that the coherence length of the fields generated in Weibel-like instabilities should be comparable to the plasma skin-depth, c/ω_p . However, magnetic power on such scales is expected to decay rapidly through collisionless phase mixing (Gruzinov 2001), while modeling of GRB afterglow observations rather indicates that magnetic fields persist over scales $\sim 10^7 - 10^9 c/\omega_p$ downstream (Gruzinov and Waxman 1999).

In a relativistic plasma, small-scale turbulence is dissipated at a damping rate⁵ $\Im\omega \simeq -k^3 c^3/\omega_p^2$ (Chang et al. 2008; Lemoine 2015) as a function of the wavenumber k , indicating that small scales are erased early on. Larger modes can survive longer; power on scales exceeding the Larmor radius of the bulk plasma decays on long, $\Im\omega \propto k^2$ MHD scales (Keshet et al. 2009). It is not clear at present whether the small-scale turbulence manages to evolve to larger scales through inverse cascade effects (*e.g.* Medvedev et al. 2005; Katz et al. 2007; Zrake 2014), whether it is dissipated but at a rate which allows to match the observations (Lemoine 2013; Lemoine et al. 2013), or whether a large-scale field is seeded in the downstream plasma by some external instabilities (*e.g.* Sironi and Goodman 2007; Couch et al. 2008; Levinson 2009).

PIC simulations have quantified the generation of upstream current filaments by pinching instabilities (*e.g.* Silva et al. 2003; Frederiksen et al. 2004; Jaroschek et al. 2005; Spitkovsky 2005, 2008a; Chang et al. 2008), and resolved the formation of shocks in two- and three-dimensional (2D and 3D) pair plasma (Spitkovsky 2005; Kato 2007; Chang et al. 2008; Keshet et al. 2009; Sironi and Spitkovsky 2009a; Haugbølle 2011; Sironi and Spitkovsky 2011b; Sironi et al. 2013) and ion-electron plasma (Spitkovsky 2008a; Martins et al. 2009; Sironi et al. 2013). These simulations revealed a rapid decay of the magnetic field downstream at early times (Gruzinov 2001; Chang et al. 2008). Yet, a slow evolution of the plasma configuration takes place on $> 10^3/\omega_p$ timescales, involving a gradual increase in the scale of the magnetic structures, and consequently their slower dissipation downstream (Keshet et al. 2009).

This long-term evolution is driven entirely by the high-energy particles accelerated in the shock; it is seen both upstream (*e.g.* in the precursor) and downstream, both of which become magnetized at increasingly large distances from the shock, and with an increasingly flat magnetic power-spectrum downstream (Keshet et al. 2009). A flatter magnetic power spectrum at the shock implies a larger fraction of the magnetic energy stored in long-wavelength modes, which may survive farther from the shock. Indeed, the index of a power-law spectrum of magnetic fluctuations directly controls how fast the magnetic energy density, integrated over wavenumbers, decays behind the shock (Chang

⁵ The shock crossing conditions imply that the relativistic plasma frequency of the shocked downstream plasma is roughly the same as the plasma frequency of the upstream plasma; no distinction will be made here between these quantities.

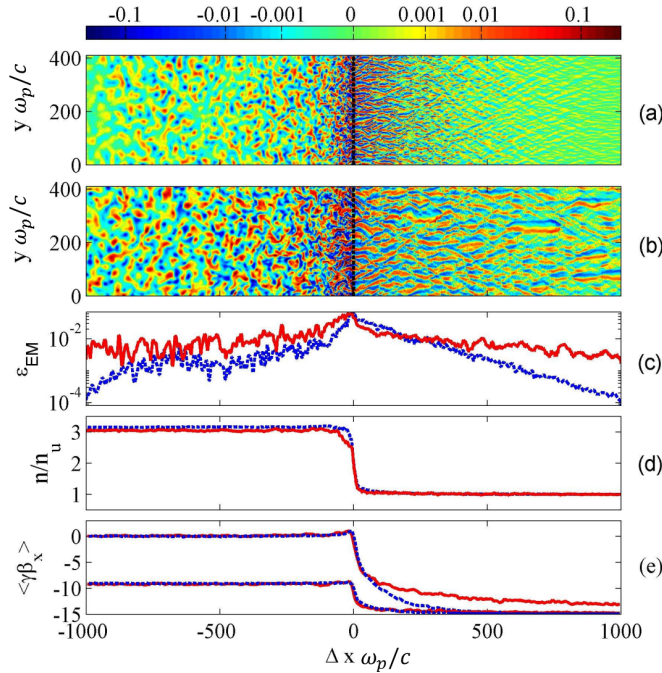


Fig. 3 Pair plasma evolution within $1000 c/\omega_p$ of the shock. The simulation is performed in the downstream frame, and the upstream flow moves with a Lorentz factor $\gamma_r = 15$ (so, γ_r is the relative Lorentz factor between the upstream and downstream regions). The normalized transverse magnetic field $\text{sign}(B) \epsilon_B$ (color scale stretched in proportion to $\epsilon_B^{1/4}$ to highlight weak features) is shown at (a) early ($t_1 = 2250 \omega_p^{-1}$), and (b) late ($t_2 = 11925 \omega_p^{-1}$) times. Here $\Delta x \equiv x - x_{\text{sh}}$ is the distance from the shock, with x_{sh} (dashed vertical line) defined as the location of median density between far upstream and far downstream. Also shown are the transverse averages (at t_1 , dashed blue, and t_2 , solid red) of (c) the electromagnetic energy $\epsilon_{EM} \equiv [(B^2 + E^2)/8\pi]/[(\gamma_r - 1)\gamma_r n' mc^2]$ (with E the electric field amplitude in the downstream frame, included in the definition of ϵ_{EM} because in the simulation frame the induced electric field in the upstream medium is $E \sim B$) normalized to the upstream kinetic energy, (d) density normalized to the far upstream density $n_u = \gamma_r n'$, and (e) particle momentum $\gamma\beta$ (with β the velocity in c units) in the x -direction averaged over all particles (higher $\langle\gamma\beta_x\rangle$) and over downstream-headed particles only.

et al. 2008; Lemoine 2015); the scale-free limit corresponds to a flat magnetic power spectrum (Katz et al. 2007).

Properly capturing the backreaction of high energy particles requires large simulation boxes and large particle numbers, to guarantee that the largest scale fields and the highest energy particles are included. The largest available simulations at the present, with length L and time T scales of $(L\omega_p/c)^2 (T\omega_p) \lesssim 10^{11}$, show no sign of convergence at $T \gtrsim 10^4 c/\omega_p$ (Keshet et al. 2009; Sironi et al. 2013). This is illustrated in Fig. 3 for a pair-plasma shock in 2D.

For magnetized shocks, the situation is different, as we describe below (Sironi et al. 2013). At strong magnetizations, and for the quasi-perpendicular

field geometry most relevant for relativistic flows, particle acceleration is suppressed, and the shock quickly reaches a steady state. At low (but nonzero) quasi-perpendicular magnetization, the shock evolves at early times similarly to the case of unmagnetized shocks (*i.e.* $\sigma = 0$). Particle acceleration proceeds to higher and higher energies, and modes of longer and longer wavelength appear. However, the maximum particle energy stops evolving once it reaches a threshold $\gamma_{sat} \propto \sigma^{-1/4}$ (Sironi et al. 2013), and at that point the overall shock structure approaches a steady state. (Sironi et al. 2013).⁶

4 PIC Simulations of Relativistic Shocks

Only in the last few years, thanks to important advances in numerical algorithms and computer capabilities, plasma simulations have been able to tackle the problem of particle acceleration in relativistic shocks from first principles. In the following, we describe the major advances driven by large-scale PIC simulations in our understanding of particle acceleration in relativistic shocks. PIC codes can model astrophysical plasmas in the most fundamental way (Birdsall and Langdon 1991; Buneman 1993; Spitkovsky 2005), as a collection of charged macro-particles that are moved by the Lorentz force. The currents deposited by the macro-particles on the computational grid are then used to solve for the electromagnetic fields via Maxwell’s equations. The loop is closed self-consistently by extrapolating the fields to the macro-particle locations, where the Lorentz force is computed.

Full PIC simulations can capture, from first principles, the acceleration physics of both electrons and ions. However, such simulations must resolve the electron plasma skin depth c/ω_{pe} , which is typically much smaller than astrophysical scales. Hence, most simulations can only cover limited time and length scales, and usually with low dimensionality (1D or 2D instead of 3D) and small ion-to-electron mass ratios (the ion skin depth c/ω_{pi} is a factor of $\sqrt{m_i/m_e}$ larger than the electron skin depth c/ω_{pe}). The results discussed below pertain to simulation durations of order $\sim 10^3 - 10^4 \omega_{pe}$ in electron-positron shocks and $\sim 10^3 \omega_{pi}$ in electron-ion shocks (but with reduced mass ratios), so a careful extrapolation is needed to bridge these microscopic scales with the macroscopic scales of astrophysical interest. Yet, as we review below, PIC simulations provide invaluable insight into the physics of particle injection and acceleration in astrophysical sources.

The structure of relativistic shocks and the efficiency of particle acceleration depend on the conditions of the upstream flow, such as bulk velocity, magnetic field strength and field orientation. PIC simulations have shown that the shock physics and the efficiency of particle acceleration are insensitive to

⁶ This conclusion regarding the saturation of the maximum particle Lorentz factor at γ_{sat} has been tested in electron-positron shocks having $\sigma = 10^{-4} - 10^{-3}$ by Sironi et al. (2013), with the largest PIC study available to date. We caution that further nonlinear evolution, beyond the timespan covered by current PIC simulations, might be present in shocks with lower magnetization.

the shock Lorentz factor (modulo an overall shift in the energy scale), in the regime $\gamma_r \gg 1$ of ultra-relativistic flows (*e.g.* Sironi et al. 2013). Below, we only discuss results for shocks where the upstream Lorentz factor with respect to the downstream frame is $\gamma_r \gtrsim 5$, neglecting the trans- and non-relativistic regimes that are outside the scope of this review. We discuss the physics of both electron-positron shocks and electron-ion shocks (up to realistic mass ratios), neglecting the case of electron-positron-ion shocks presented by *e.g.* Hoshino et al. (1992); Amato and Arons (2006); Stockem et al. (2012), which might be relevant for PWNe. As found by Sironi and Spitkovsky (2009a, 2011b); Sironi et al. (2013), for highly relativistic flows, the main parameter that controls the shock physics is the magnetization σ . Below, we distinguish between shocks propagating into strongly magnetized media ($\sigma \gtrsim 10^{-3}$) and weakly magnetized or unmagnetized shocks ($\sigma \lesssim 10^{-3}$).

4.1 Particle Acceleration in Strongly Magnetized Shocks

For high magnetizations ($\sigma \gtrsim 10^{-3}$ in electron-positron flows, or $\sigma \gtrsim 3 \times 10^{-5}$ in electron-ion flows), the shock structure and acceleration properties depend critically on the inclination angle θ between the upstream field and the shock direction of propagation (Sironi and Spitkovsky 2009a, 2011b). If the magnetic obliquity is larger than a critical angle θ_{crit} , charged particles would need to move along the field faster than the speed of light in order to outrun the shock (“superluminal” configurations). In Fig. 4, we show how the critical angle θ_{crit} (as measured in the downstream frame) depends on the flow velocity and magnetization. In the limit of $\sigma \ll 1$ and $\gamma_r \gg 1$, the critical obliquity approaches the value $\theta_{\text{crit}} \simeq 34^\circ$.

Only “subluminal” shocks ($\theta \lesssim \theta_{\text{crit}}$) are efficient particle accelerators (Sironi and Spitkovsky 2009a, 2011b; Sironi et al. 2013), in agreement with the analytical findings of Begelman and Kirk (1990). As illustrated in Fig. 5, a stream of shock-accelerated particles propagates ahead of the shock (panel (c)), and their counter-streaming with the incoming flow generates magnetic turbulence in the upstream region (panel (b)). In turn, such waves govern the acceleration process, by providing the turbulence required for the Fermi mechanism. In the particular case of Fig. 5 — a relativistic shock with $\gamma_r = 15$, $\sigma = 0.1$ and $\theta = 15^\circ$ propagating into an electron-ion plasma — the upstream turbulence is dominated by Bell-like modes (Reville et al. 2006; Lemoine and Pelletier 2010, 2011). The downstream particle spectrum in subluminal shocks shows a pronounced non-thermal tail of shock-accelerated particles with a power-law index $2 \lesssim s_\gamma \lesssim 3$ (panel (d)). The tail contains $\sim 5\%$ of the particles and $\sim 20\%$ of the flow energy at time $2250 \omega_{\text{pi}}^{-1}$; both values appear to be time-converged, within the timespan covered by our simulations.

In contrast, superluminal shocks ($\theta \gtrsim \theta_{\text{crit}}$) show negligible particle acceleration (Gallant et al. 1992; Hoshino 2008; Sironi and Spitkovsky 2009a, 2011b; Sironi et al. 2013). Here, due to the lack of significant self-generated turbulence, charged particles are forced to slide along the background field lines,

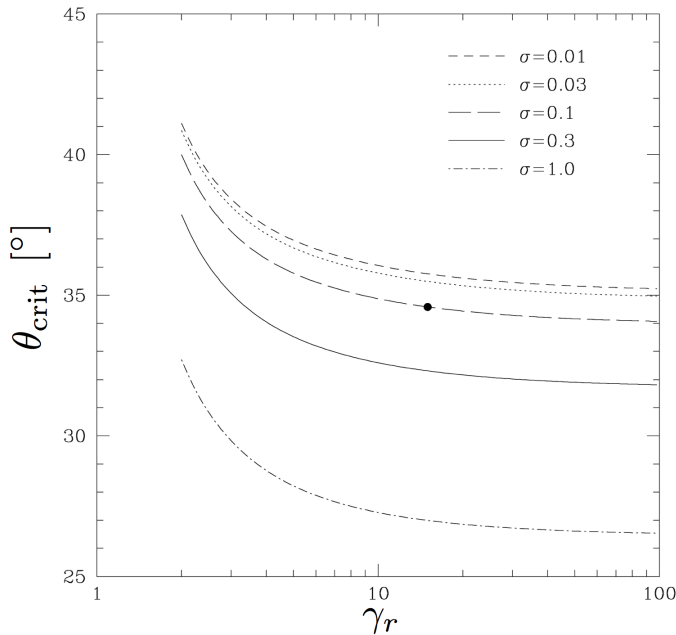


Fig. 4 Critical obliquity angle θ_{crit} (measured in the downstream frame) that separates subluminal and superluminal configurations (Sironi and Spitkovsky 2009a), as a function of the flow Lorentz factor γ_r and the magnetization σ , as indicated in the label. The filled black circle indicates our reference case with $\gamma_r = 15$ and $\sigma = 0.1$.

whose orientation prohibits repeated crossings of the shock. This inhibits the Fermi process, and in fact the particle distribution behind superluminal shocks is purely thermal. The same conclusion holds for both electron-positron and electron-ion flows. In electron-ion shocks, the incoming electrons are heated up to the ion energy, due to powerful electromagnetic waves emitted by the shock into the upstream medium, as a result of the synchrotron maser instability (studied analytically by Lyubarsky (2006), and with 1D PIC simulations by *e.g.* Langdon et al. (1988); Gallant et al. (1992); Hoshino et al. (1992); Hoshino (2008)). Yet, such heating is not powerful enough to permit an efficient injection of electrons into the Fermi acceleration process at superluminal electron-ion shocks.

If magnetized superluminal shocks are responsible for producing the radiating particles in astrophysical relativistic sources, the strong electron heating observed in electron-ion shocks implies that the putative power-law tail in the electron spectrum should start from energies higher than the ion bulk kinetic energy. For models of GRBs and AGN jets that require a power-law distribution extending down to lower energies, the presence of such shocks would suggest that electron-positron pairs may be a major component of the flow.

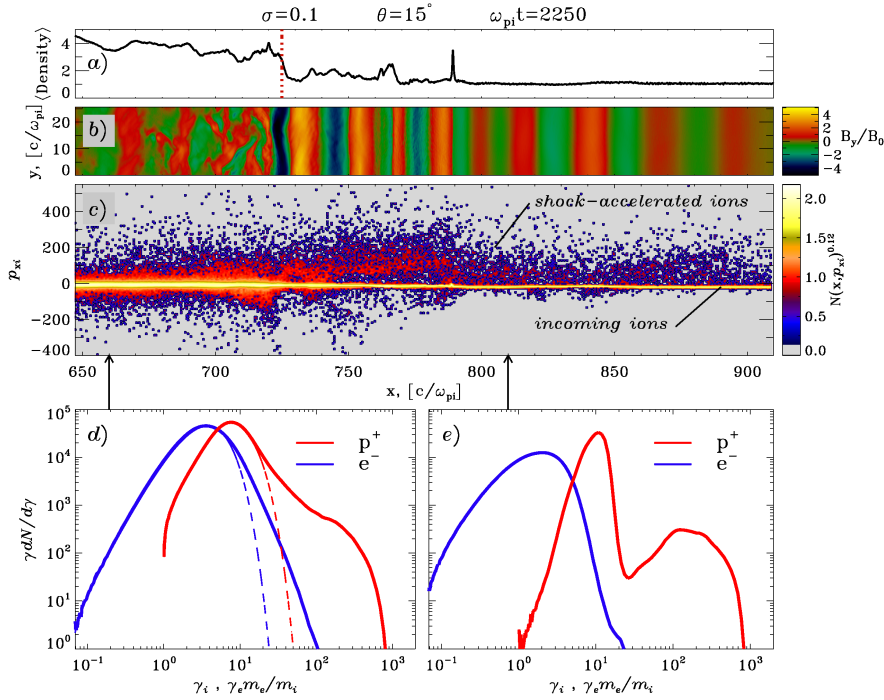


Fig. 5 Structure of an electron-ion subluminal shock with $\gamma_r = 15$, $\sigma = 0.1$ and $\theta = 15^\circ$, from [Sironi and Spitkovsky \(2011b\)](#). The simulation is performed in the downstream frame. The shock front is located at $x \sim 725 c/\omega_{pi}$ (vertical dotted red line in panel (a)), and it separates the upstream region (to its right) from the compressed downstream region (to its left). A stream of shock-accelerated ions propagates ahead of the shock (see the diffuse cloud in the momentum space $x - p_{xi}$ of panel (c) to the right of the shock, at $x \gtrsim 725 c/\omega_{pi}$). Their interaction with the upstream flow (narrow beam to the right of the shock in panel (c)) generates magnetic turbulence ahead of the shock (see the transverse waves in panel (b), to the right of the shock). In turn, such waves govern the process of particle acceleration. In fact, the particle spectrum behind the shock (solid lines in panel (d); red for ions, blue for electrons) is not compatible with a simple thermal distribution (dashed lines), showing a clear non-thermal tail of high-energy particles, most notably for ions.

4.2 Particle Acceleration in Weakly Magnetized and Unmagnetized Shocks

Weakly magnetized shocks ($\sigma \lesssim 10^{-3}$ in electron-positron flows, $\sigma \lesssim 3 \times 10^{-5}$ in electron-ion flows) are governed by electromagnetic plasma instabilities (see §3.1), that generate magnetic fields stronger than the background field. Such shocks do accelerate particles self-consistently, regardless of the magnetic obliquity angle ([Spitkovsky 2008a,b](#); [Martins et al. 2009](#); [Haugbølle 2011](#); [Sironi et al. 2013](#)). The stream of shock-accelerated particles propagates ahead of the shock, triggering the Weibel instability. The instability generates filamentary magnetic structures in the upstream region, as shown in [Fig. 6](#), which

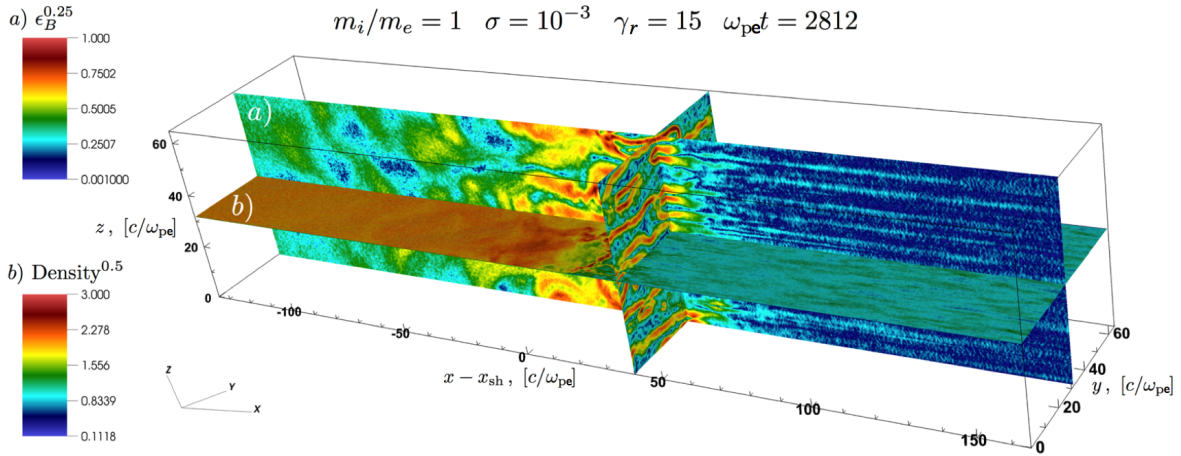


Fig. 6 Shock structure from the 3D PIC simulation of a $\sigma = 10^{-3}$ electron-positron shock with $\gamma_r = 15$, from [Sironi et al. \(2013\)](#). The simulation is performed in the downstream frame and the shock propagates along $+\hat{x}$. We show the xy slice of the particle number density (normalized to the upstream density), and the xz and yz slices of the magnetic energy fraction ϵ_B . A stream of shock-accelerated particles propagates ahead of the shock, and their counter-streaming motion with respect to the incoming flow generates magnetic turbulence in the upstream via electromagnetic micro-instabilities. In turn, such waves provide the scattering required for particle acceleration.

in turn scatter the particles back and forth across the shock, mediating Fermi acceleration.

The accelerated particles in weakly magnetized shocks populate in the downstream region a power-law tail $dN/d\gamma \propto \gamma^{-s_\gamma}$ with a slope $s_\gamma \sim 2.5$, that contains $\sim 3\%$ of the particles and $\sim 10\%$ of the flow energy.⁷ In electron-ion shocks, the acceleration process proceeds similarly for the two species, since the electrons enter the shock nearly in equipartition with the ions, as a result of strong pre-heating in the self-generated Weibel turbulence ([Spitkovsky 2008a](#); [Martins et al. 2009](#); [Sironi et al. 2013](#)). In both electron-positron and electron-ion shocks, the maximum energy of the accelerated particles scales in time as $\gamma_{max} \propto t^{1/2}$ ([Sironi et al. 2013](#)), as shown in [Fig. 7](#). More precisely, the maximum particle Lorentz factor in the downstream frame scales as

$$\gamma_{max} \simeq 0.5 \gamma_r (\omega_{pe} t)^{1/2} \quad (4)$$

$$\gamma_{max,i} \sim \frac{\gamma_{max,e} m_e}{m_i} \simeq 0.25 \gamma_r (\omega_{pi} t)^{1/2} \quad (5)$$

in electron-positron and in electron-ion shocks, respectively ([Sironi et al. 2013](#)). This scaling is shallower than the so-called (and commonly assumed) Bohm

⁷ These values are nearly independent of the flow composition and magnetization, in the regime of weakly magnetized shocks. Also, they are measured at time $\sim 10^4 \omega_{pe}^{-1}$ in electron-positron shocks and at $\sim 10^3 \omega_{pi}^{-1}$ in electron-ion shocks, but they appear remarkably constant over time, within the timespan covered by our simulations.

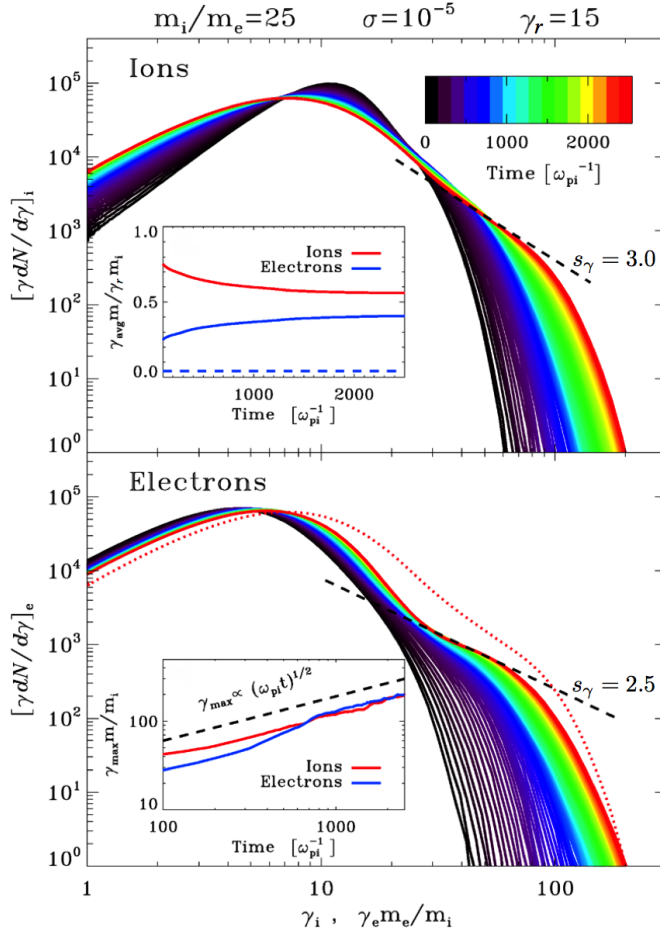


Fig. 7 Temporal evolution of the downstream particle spectrum, from the 2D simulation of a $\gamma_r = 15$ electron-ion ($m_i/m_e = 25$) shock propagating into a flow with magnetization $\sigma = 10^{-5}$, from Sironi et al. (2013). The evolution of the shock is followed from its birth (black curve) up to $\omega_{pi}t = 2500$ (red curve). In the top panel we show the ion spectrum and in the bottom panel the electron spectrum. The non-thermal tails approach at late times a power law with a slope $s_\gamma = 3.0$ for ions and $s_\gamma = 2.5$ for electrons (black dashed lines in the two panels). In the bottom panel, we overplot the ion spectrum at $\omega_{pi}t = 2500$ with a red dotted line, showing that ions and electrons are nearly in equipartition. Inset of the top panel: mean downstream ion (red) and electron (blue) energy, in units of the bulk energy of an upstream particle. The dashed blue line shows the electron energy at injection. Inset of the bottom panel: temporal evolution of the maximum Lorentz factor of ions (red) and electrons (blue), scaling as $\propto (\omega_{pi}t)^{1/2}$ at late times (black dashed line).

limit $\gamma_{max} \propto t$, and it naturally results from the small-scale nature of the Weibel turbulence generated in the shock layer (see Fig. 6).

The increase of the maximum particle energy over time proceeds up to a saturation Lorentz factor (once again, measured in the downstream frame)

that is constrained by the magnetization σ of the upstream flow

$$\gamma_{sat} \simeq 4 \gamma_r \sigma^{-1/4} \quad (6)$$

$$\gamma_{sat,i} \sim \frac{\gamma_{sat,e} m_e}{m_i} \simeq 2 \gamma_r \sigma^{-1/4} \quad (7)$$

in electron-positron and electron-ion shocks, respectively. The saturation of the maximum particle energy is shown in Fig. 8 for a shock with $\sigma = 10^{-3}$. Further energization is prevented by the fact that the self-generated turbulence is confined within a region of thickness $L_{B,sat} \propto \sigma^{-1/2}$ around the shock (Sironi et al. 2013).

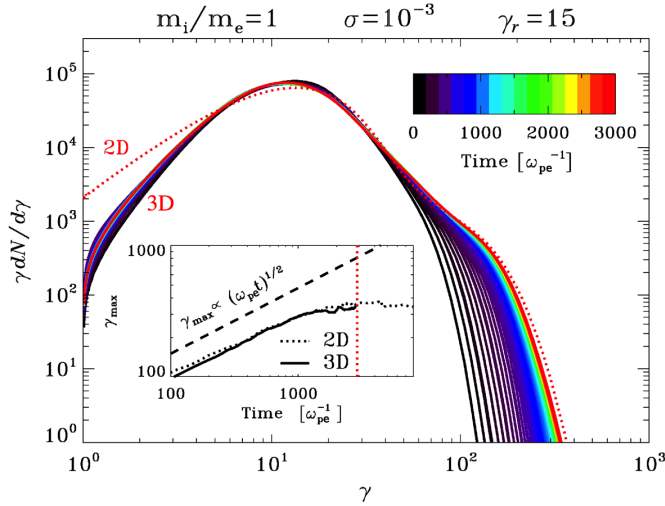


Fig. 8 Time evolution of the downstream particle spectrum from the 3D PIC simulation of a $\sigma = 10^{-3}$ electron-positron shock with $\gamma_r = 15$, from Sironi et al. (2013). The evolution of the shock is followed from its birth (black curve) up to $\omega_{pe}t = 3000$ (red curve). We overplot the spectrum at $\omega_{pe}t = 3000$ from a 2D simulation with the same parameters (red dotted line), showing excellent agreement at high energies. The inset shows that the maximum particle Lorentz factor grows as $\gamma_{max} \propto t^{1/2}$, before saturating at $\gamma_{sat} \propto \sigma^{-1/4}$. The results are consistent between 2D (dotted) and 3D (solid).

5 Astrophysical Implications

5.1 Acceleration of Ultra-High Energy Cosmic Rays

Relativistic shock waves have long been considered as prime candidates for the acceleration of cosmic rays to the highest energies observed, $E \sim 10^{20}$ eV. Indeed, a naive extrapolation of the acceleration time scale in the sub-relativistic regime ($t_{acc} \sim t_{scatt}/\beta_u^2$, with t_{scatt} the scattering timescale) suggests that relativistic shocks (*i.e.* $\beta_u \sim 1$) accelerate particles on shorter time scales than

non-relativistic shocks (*i.e.* $\beta_u \ll 1$), at a given t_{scatt} . For given radiative loss and escape time scales, this implies that relativistic shocks would be accelerating particles to much higher energies than non-relativistic shocks. However, the situation is more complex than it appears; in particular, in relativistic shock waves, t_{scatt} may be much larger than usually assumed.

As mentioned repeatedly in the previous paragraphs, particle acceleration in the relativistic regime $\gamma_u \beta_u \gg 1$ around a steady planar shock wave, operates only if intense micro-turbulence has been excited in the shock precursor, as demonstrated analytically (Lemoine et al. 2006), by Monte Carlo simulations (Niemiec et al. 2006) and by PIC simulations (Sironi et al. 2013); consequences for the acceleration of particles to ultra-high energies have been discussed in several papers, *e.g.* by Pelletier et al. (2008), Lemoine and Waxman (2009), Lemoine (2011), Eichler and Pohl (2011), Bykov et al. (2012); Sironi et al. (2013) or more recently by Reville and Bell (2014).

Scattering in small-scale turbulence leads to a downstream residence time $t_{\text{scatt}} \sim r_L^2 / (\lambda_{\delta B} c)$, with r_L the Larmor radius of the particle and $\lambda_{\delta B}$ the coherence length scale of the turbulence. This implies that the (shock frame) acceleration timescale t_{acc} grows quadratically with the energy, which fits well the result seen in PIC simulations that the maximum energy grows as the square root of time. In other words, as the particle energy grows, the acceleration timescale departs more and more from the Bohm estimate, which is generally used to compute the maximum energy. Comparing for instance the acceleration timescale, which is at least equal to the above downstream residence time, with the dynamical timescale r/γ_u in the shock rest frame (r denoting the radius of the shock front in the upstream rest frame), one finds a maximum energy $E_{\text{max}} \lesssim e \delta B r (\gamma_u \lambda_{\delta B} / r)^{1/2}$, with δB the strength of the turbulent field expressed in the shock frame; the above maximal energy has been written in the upstream (observer) frame. The factor in the brackets generally takes very small values, because $\lambda_{\delta B} \sim c/\omega_p$ while r is a macroscopic length scale; this maximal energy is thus far below the so-called Hillas estimate $e \delta B r$, which corresponds to a Bohm estimate for t_{scatt} .

Another way to phrase the problem is as follows (see Lemoine and Waxman 2009 for a discussion): assume that the acceleration timescale is written $t_{\text{acc}} = \mathcal{A} r_L / c$, and derive the maximum energy by comparing t_{acc} with $t_{\text{dyn}} = r / (\gamma \beta c)$ as above for a jet moving at velocity β towards the observer. Then one finds that acceleration of particles of charge Z to $10^{20} E_{20}$ eV requires that the isotropic equivalent magnetic luminosity of the object exceeds: $L_B \gtrsim 10^{45} Z^{-2} E_{20}^2 \mathcal{A}^2 \gamma^2$ erg/s, a very large number indeed, all the more so if $\mathcal{A} \gg 1$. For acceleration at ultra-relativistic shock waves, \mathcal{A} is much larger than unity (while the Bohm estimate corresponds to $\mathcal{A} \sim 1$), with typical values $\mathcal{A} \sim E / (\gamma_u m_p c^2)$. In summary, particle acceleration at ultra-relativistic shock waves does not appear fast enough to produce particles of ultra-high energies. In particular, when the above arguments are applied to the case of the external shock of a GRB, the maximal energy is found to be of the order of 10^{16} eV (Plotnikov et al. 2013; Sironi et al. 2013; Reville and Bell 2014).

It is important however to note three caveats in the above arguments. One is that as $\gamma_u \beta_u \rightarrow 1$, *i.e.* for mildly relativistic shock waves, the nature of the turbulence remains unknown and one cannot exclude that scattering would be closer to a Bohm estimate. Two facts support such a speculation: (1) the precursor increases in size as γ_u diminishes, which suggests that MHD-scale instabilities could arise and excite large scale turbulence; and (2), the obliquity becomes less of a problem for mildly relativistic shock waves, suggesting that large scale turbulence could possibly lead to acceleration in this regime. A second caveat is the fact that PWNe are very efficient particle accelerators, even though one would expect the opposite in the absence of reconnection or other dissipative processes, due to the large magnetization of the flow (Section 5.3). More precisely, synchrotron photons are observed with energies as high as 100 MeV, which means that pairs are accelerated up to the radiation-reaction limit, *i.e.* with an acceleration time scale close to the theoretical Bohm scaling. Such empirical evidence suggests that ions could also be accelerated to very high energies, if ions are indeed injected along with pairs in the wind. In the Crab, such a maximal energy would be limited by the confinement in the nebular turbulence to values of the order of 10^{17} eV (for $Z = 1$); more powerful nebulae, associated with young pulsars born with a few millisecond periods, could however confine (and potentially accelerate) protons up to the highest energies (Lemoine et al. 2014). Finally, as the nonlinear evolution of weakly magnetized or parallel shocks over long timescales is not yet understood, some of the above estimates, pertaining *e.g.* to the diffusive properties and extent of the magnetic field, may be altered on macroscopic times.

5.2 Radiative Signatures of Relativistic Blast Waves

In line with the previous discussion, one can compute the maximal energy for electrons and derive the maximal synchrotron photon energy. Using an acceleration time scale $t_{\text{acc}} \simeq r_L^2 / (\lambda_{\delta} B c)$ and comparing to synchrotron losses in the self-generated micro-turbulence, characterized by its magnetization ϵ_B , one derives a maximum synchrotron photon energy of the order of a few GeV in the early phase of GRB afterglows, *i.e.* during the first hundreds of seconds (Kirk and Reville 2010; Plotnikov et al. 2013; Lemoine 2013; Wang et al. 2013; Sironi et al. 2013). Let us stress that in the latter study, this estimate has been derived from PIC simulations with a self-consistent measurement of the acceleration time scale in the self-consistent magnetic field. The synchrotron radiation of electrons accelerated at the external ultra-relativistic shock of GRBs can thus produce the bulk of the long-lasting > 100 MeV emission detected by the Fermi satellite (*e.g.* Kumar and Barniol Duran 2009; Ackermann 2010; De Pasquale 2010; Ghisellini et al. 2010). The photons that have been observed with energies in excess of $\gtrsim 10$ GeV probably result from inverse Compton interactions (Wang et al. 2013). Interestingly, the recent GRB130427A has revealed a long-lasting emission with a possible break in the spectrum at an energy of a GeV, characteristic of a turn-over between the synchrotron and the

synchrotron self-Compton components (Tam et al. 2013), in good qualitative agreement with the above arguments.

Other potential radiative signatures of the shock microphysics come from the small-scale nature of the turbulence and its long-term evolution in the blast. As discussed in Section 3.2, one notably expects this turbulence to relax through collisionless damping on hundreds of c/ω_p (Chang et al. 2008; Keshet et al. 2009; Lemoine 2015) while the electrons typically cool on much longer length scales. In GRB external blast waves, the shocked region is typically 7–9 orders of magnitude larger than c/ω_p in size, which leaves room for a substantial evolution of ϵ_B , even if it decreases as a mild power-law in distance from the shock, as suggested by the above studies. Since the electron cooling length depends on the inverse of the electron Lorentz factor, particles of different initial Lorentz factors emit their energy in regions of different magnetic field strength, leading to a non-standard synchrotron spectrum (Rossi and Rees 2003; Derishev 2007; Lemoine 2013), which could in principle be used as a tomograph of the evolution of the micro-turbulence downstream of the shock. Interestingly, in this picture the decay index of the turbulence is related to the long-wavelength content of the power spectrum of magnetic fluctuations at the shock front, which is unknown so far, as it is known to be modified by the acceleration of higher energy particles (Keshet et al. 2009). Finally, it is interesting to note that the recent broad-band analysis of GRB afterglows seen from the radio up to GeV energies has indeed revealed spectral signatures of a decaying magnetic field (Lemoine et al. 2013), with a decay law scaling with distance from the shock roughly as $\Delta x^{-0.5}$ (Δx being the proper distance to the shock in the downstream frame).

As discussed in Section 3.2, there are alternative possibilities however; it has been suggested for instance that the turbulence could evolve in a self-similar way as a function of distance to the shock, maintaining a uniform ϵ_B thanks to an inverse cascade process (Katz et al. 2007). It is also possible that external sources seed the blast with a large scale long-lived turbulence, *e.g.* through a Rayleigh-Taylor instability at the contact discontinuity (Levinson 2009) or through small scale dynamos following the interaction of the shock front with external inhomogeneities (Sironi and Goodman 2007; Couch et al. 2008). Hopefully, future high accuracy observational data will provide diagnostics which can be confronted with numerical simulations.

The possibility that the small scale nature of the turbulence gives rise to diffusive (or jitter) synchrotron radiation rather than conventional synchrotron radiation has also attracted attention (*e.g.* Medvedev 2000, 2006; Fleishman 2006; Mao and Wang 2011; Medvedev et al. 2011; Kelner et al. 2013). In particular, jitter radiation has been proposed as a solution for the fact that GRBs prompt spectra below the peak frequency are not always compatible with the predictions of synchrotron emission (the so-called “line of death” puzzle, see Preece (1998)). In the jitter regime, particles are deflected by less than $1/\gamma$ (γ is the electron Lorentz factor) as they cross a wavelength $\lambda_{\delta B}$, implying that coherence of the emission is maintained over several coherence cells of the turbulence. This regime thus takes place whenever the wiggler parame-

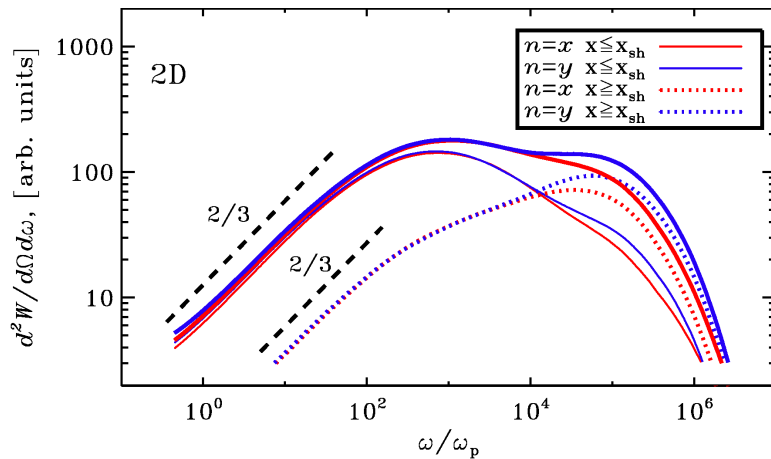


Fig. 9 *Ab initio* photon spectrum (thick solid lines) from the 2D PIC simulation of an unmagnetized (*i.e.* $\sigma = 0$) pair shock. Red lines are for head-on emission ($\hat{n} = \hat{x}$, along the shock direction of propagation), blue lines for edge-on emission ($\hat{n} = \hat{y}$, along the shock front). The slope at low frequencies is $2/3$ (black long-dashed lines), proving that the spectra are consistent with synchrotron radiation from a 2D particle distribution (in 3D, the predicted slope of $1/3$ is obtained). By separating the relative contribution of downstream ($x \leq x_{\text{sh}}$; thin solid lines) and upstream ($x \geq x_{\text{sh}}$; dotted lines) particles, one sees that upstream particles contribute significantly to the total emission (thick solid lines), especially at high frequencies. Frequencies are in units of the plasma frequency ω_p .

ter $a \equiv e\delta B\lambda_{\delta B}/mc^2 \ll 1$, while the standard synchrotron approximation becomes valid in the opposite limit. However, it is easy to verify that in the vicinity of the shock $a \sim \bar{\gamma}_{\text{sh}}$, with $\bar{\gamma}_{\text{sh}}$ the average Lorentz factor of the supra-thermal electrons in the shock rest frame, suggesting that jitter signatures must be weak.

The absence of jitter radiation in relativistic shocks has been demonstrated from first principles by computing the radiation from particles in PIC simulations (Sironi and Spitkovsky 2009b), which produce spectra entirely consistent with synchrotron radiation in the fields generated by the Weibel instability (Fig. 9). The so-called “jitter” regime is recovered only by artificially reducing the strength of the fields, such that the parameter a becomes much smaller than unity. So, if the GRB prompt emission results from relativistic unmagnetized shocks, it seems that resorting to the jitter regime is not a viable solution for the “line of death” puzzle. At frequencies above the peak, the synthetic spectra from PIC simulations show, somewhat unexpectedly, that the contribution of the upstream medium to the total emission is not negligible (Fig. 9), yet it is omitted in most models. This causes the radiation spectrum to be flatter than the corresponding downstream spectrum, thus partly masking the contribution of downstream thermal particles.

5.3 Radiative Signatures of Pulsar Wind Nebulae

The spectrum of PWNe consists of two components, where the low energy component, most likely dominated by synchrotron, shows a cutoff at a few tens of MeV. The fact that synchrotron emission reaches these energies, despite the rapid synchrotron cooling, implies that particle acceleration in the nebula is an extremely fast process (de Jager and Harding 1992), which challenges our understanding of particle acceleration in relativistic shocks.

Around the equatorial plane of obliquely-rotating pulsars, the wind consists of toroidal stripes of opposite magnetic polarity, separated by current sheets of hot plasma. It is still a subject of active research whether the alternating stripes will dissipate their energy into particle heat ahead of the termination shock, or whether the wind remains dominated by Poynting flux till the termination shock (Lyubarsky and Kirk 2001; Kirk and Skjæraasen 2003; Sironi and Spitkovsky 2011a). If the stripes are dissipated far ahead of the termination shock, the upstream flow is weakly magnetized and the pulsar wind reaches a terminal Lorentz factor (in the frame of the nebula) $\gamma_r \sim L_{sd}/m_e c^2 \dot{N} \simeq 3.7 \times 10^4 L_{sd,38.5} \dot{N}_{40}^{-1}$, where $L_{sd} \equiv 3 \times 10^{38} L_{sd,38.5}$ ergs s⁻¹ is the spin-down luminosity of the Crab (the Crab Nebula is the prototype of PWNe), and $\dot{N} = 10^{40} \dot{N}_{40}$ s⁻¹ is the particle flux entering the nebula, including the radio-emitting electrons (Bucciantini et al. 2011).

For electron-positron flows, as appropriate for pulsar winds, the maximum particle Lorentz factor in the downstream frame increases with time as $\gamma_{max} \sim 0.5 \gamma_r (\omega_p t)^{1/2}$ (see Section 4). The plasma frequency ω_p can be computed from the number density ahead of the termination shock, which is $n_{TS} = \dot{N}/(4\pi R_{TS}^2 c)$, assuming an isotropic particle flux. Here, $R_{TS} \equiv 3 \times 10^{17} R_{TS,17.5}$ cm is the termination shock radius. Balancing the acceleration rate with the synchrotron cooling rate in the self-generated Weibel fields, the maximum electron Lorentz factor is

$$\gamma_{sync,e} \simeq 3.5 \times 10^8 L_{sd,38.5}^{1/6} \dot{N}_{40}^{-1/3} \epsilon_{B,-2.5}^{-1/3} R_{TS,17.5}^{1/3}. \quad (8)$$

A stronger constraint comes from the requirement that the diffusion length of the highest energy electrons be smaller than the termination shock radius (*i.e.* a confinement constraint). Alternatively, the acceleration time should be shorter than R_{TS}/c , which yields the critical limit

$$\gamma_{conf,e} \simeq 1.9 \times 10^7 L_{sd,38.5}^{3/4} \dot{N}_{40}^{-1/2}, \quad (9)$$

which is generally more constraining than the cooling-limited Lorentz factor $\gamma_{sync,e}$. The corresponding synchrotron photons will have energies

$$h\nu_{conf,e} \simeq 0.17 L_{sd,38.5}^2 \dot{N}_{40}^{-1} \epsilon_{B,-2.5}^{1/2} R_{TS,17.5}^{-1} \text{ keV} \quad (10)$$

which are apparently too small to explain the X-ray spectrum of the Crab, extending to energies beyond a few tens of MeV. We conclude that Fermi acceleration at the termination shock of PWNe is not a likely candidate for

producing X-ray photons via the synchrotron process, and valid alternatives should be investigated.

One possibility – magnetic dissipation of the striped pulsar wind in and around the shock front itself – has been extensively studied, with the conclusion that particle acceleration along extended X-lines formed by tearing of the current sheets may contribute to the flat particle distribution (with spectral index $s_\gamma \simeq 1.5$) required to explain the far infrared and radio spectra of PWNe (*e.g.*, Lyubarsky 2003; Sironi and Spitkovsky 2011a, 2012). Indeed, hard particle spectra are found to be a generic by-product of magnetic reconnection in the relativistic regime appropriate for pulsar winds (Sironi and Spitkovsky 2014; Sironi et al. 2015, see also Kagan et al. (2015) in the present volume). However, further acceleration to gamma-ray emitting energies by the Fermi process cannot occur in the shock that terminates the pulsar wind, if particle scattering depends only on the self-generated turbulence.

Yet, the steady-state hard X-ray and gamma-ray spectra of PWNe do look like the consequences of Fermi acceleration – particle distributions with $s_\gamma \simeq 2.4$ are implied by the observations. In this regard, we argue that the wind termination shock might form in a macroscopically turbulent medium, with the outer scale of the turbulence driven by the large-scale shear flows in the nebula (Komissarov and Lyubarsky 2004; Del Zanna et al. 2004; Camus et al. 2009). If the large-scale motions drive a turbulent cascade to shorter wavelengths, back-scattering of the particles in this downstream turbulence, along with upstream reflection by the transverse magnetic field of the wind, might sustain Fermi acceleration to higher energies.

Another “external” influence of reconnection on the shock structure, that might lead to particle acceleration to higher energies, may be connected to the accelerator behind the recently discovered gamma-ray flares in the Crab Nebula (Abdo 2011). Runaway acceleration of electrons and positrons at reconnection X-lines, a linear accelerator, may inject energetic beams into the shock, with the mean energy per particle approaching the whole open field line voltage, $\gtrsim 10^{16}$ V in the Crab (Arons 2012), as required to explain the Crab GeV flares. This high-energy population can drive cyclotron turbulence when gyrating in the shock-compressed fields, and resonant absorption of the cyclotron harmonics can accelerate the electron-positron pairs in a broad spectrum, with maximum energy again comparable to the whole open field line voltage (Hoshino et al. 1992; Amato and Arons 2006).

6 Conclusions

There has been significant progress in our understanding of relativistic shocks in recent years, thanks to both analytical work and numerical simulations. The highly nonlinear problem of particle acceleration and magnetic field generation in shocks — with the accelerated particles generating the turbulence that in turn mediates their acceleration — is being tackled from first principles, assessing the parameter regime where particle acceleration in relativistic shocks

is efficient. In this chapter, we have described the basic analytical formalism of test particle acceleration in relativistic shocks, leading to the “universal” energy slope $s_\gamma \simeq 2.2$ in the ultra-relativistic limit; we have unveiled the most relevant plasma instabilities that mediate injection and acceleration in relativistic shocks; and we have summarized recent results of large-scale PIC simulations concerning the efficiency and rate of particle acceleration in relativistic shocks, and the long-term evolution of the self-generated magnetic turbulence. Our novel understanding of particle acceleration and magnetic field generation in relativistic shocks has profound implications for the modeling of relativistic astrophysical sources, most importantly PWNe, GRBs, and AGN jets.

Acknowledgments: We gratefully thank Boaz Katz, Guy Pelletier, Anatoly Spitkovsky and Eli Waxman for their collaboration on many of the issues discussed here. U.K. is supported by the European Union Seventh Framework Programme (FP7/2007-2013) under grant agreement n° 293975, by an IAEC-UPBC joint research foundation grant, and by an ISF-UGC grant. M.L. acknowledges support by the ANR-14-CE33-0019 MACH project.

References

- A.A. Abdo, Gamma-Ray Flares from the Crab Nebula. *Science* **331**, 739 (2011). doi:10.1126/science.1199705
- A. Achterberg, J. Wiersma, The Weibel instability in relativistic plasmas. I. Linear theory. *A&Ap* **475**, 1–18 (2007). doi:10.1051/0004-6361:20065365
- A. Achterberg, J. Wiersma, C.A. Norman, The Weibel instability in relativistic plasmas. II. Nonlinear theory and stabilization mechanism. *A&Ap* **475**, 19–36 (2007). doi:10.1051/0004-6361:20065366
- A. Achterberg, Y.A. Gallant, J.G. Kirk, A.W. Guthmann, Particle acceleration by ultrarelativistic shocks: theory and simulations. *Mon. Not. R. Astron. Soc.* **328**, 393–408 (2001). doi:10.1046/j.1365-8711.2001.04851.x
- M. Ackermann, Fermi Observations of GRB 090510: A Short-Hard Gamma-ray Burst with an Additional, Hard Power-law Component from 10 keV TO GeV Energies. *Astrophys. J.* **716**, 1178–1190 (2010). doi:10.1088/0004-637X/716/2/1178
- E. Amato, J. Arons, Heating and Nonthermal Particle Acceleration in Relativistic, Transverse Magnetosonic Shock Waves in Proton-Electron-Positron Plasmas. *Astrophys. J.* **653**, 325–338 (2006). doi:10.1086/508050
- J. Arons, Pulsar Wind Nebulae as Cosmic Pevatrons: A Current Sheet’s Tale. *Space Sci. Rev.* **173**, 341–367 (2012). doi:10.1007/s11214-012-9885-1
- J. Arons, M. Tavani, Relativistic particle acceleration in plerions. *Astrophys. J. Supp.* **90**, 797–806 (1994). doi:10.1086/191905
- W.I. Axford, E. Leer, G. Skadron, Acceleration of cosmic rays by shock waves., in *Cosmophysics*, ed. by V.A. Dergachev, G.E. Kocharov, 1978, pp. 125–134
- J. Bednarz, M. Ostrowski, Energy Spectra of Cosmic Rays Accelerated at Ultrarelativistic Shock Waves. *Physical Review Letters* **80**, 3911–3914 (1998). doi:10.1103/PhysRevLett.80.3911
- M.C. Begelman, J.G. Kirk, Shock-drift particle acceleration in superluminal shocks - A model for hot spots in extragalactic radio sources. *Astrophys. J.* **353**, 66–80 (1990). doi:10.1086/168590
- A.R. Bell, The acceleration of cosmic rays in shock fronts. I. *Mon. Not. R. Astron. Soc.* **182**, 147–156 (1978)

- E. Berger, S.R. Kulkarni, D.A. Frail, A Standard Kinetic Energy Reservoir in Gamma-Ray Burst Afterglows. *Astrophys. J.* **590**, 379–385 (2003). doi:10.1086/374892
- C.K. Birdsall, A.B. Langdon, *Plasma Physics via Computer Simulation* 1991
- R. Blandford, D. Eichler, Particle Acceleration at Astrophysical Shocks - a Theory of Cosmic-Ray Origin. *Physics Reports* **154**, 1 (1987). doi:10.1016/0370-1573(87)90134-7
- R.D. Blandford, J.P. Ostriker, Particle acceleration by astrophysical shocks. *Astrophys. J. Lett.* **221**, 29–32 (1978). doi:10.1086/182658
- P. Blasi, M. Vietri, On Particle Acceleration around Shocks. II. A Fully General Method for Arbitrary Shock Velocities and Scattering Media. *Astrophys. J.* **626**, 877–886 (2005). doi:10.1086/430164
- A. Bret, Weibel, Two-Stream, Filamentation, Oblique, Bell, Buneman...Which One Grows Faster? *Astrophys. J.* **699**, 990–1003 (2009). doi:10.1088/0004-637X/699/2/990
- A. Bret, L. Gremillet, D. Bénisti, Exact relativistic kinetic theory of the full unstable spectrum of an electron-beam-plasma system with Maxwell-Jüttner distribution functions. *Phys. Rev. E* **81**(3), 036402 (2010). doi:10.1103/PhysRevE.81.036402
- N. Bucciantini, J. Arons, E. Amato, Modelling spectral evolution of pulsar wind nebulae inside supernova remnants. *Mon. Not. R. Astron. Soc.* **410**, 381–398 (2011). doi:10.1111/j.1365-2966.2010.17449.x
- O. Buneman, in “*Computer Space Plasma Physics*”, *Terra Scientific, Tokyo*, 67, 1993
- A.M. Bykov, R.A. Treumann, Fundamentals of collisionless shocks for astrophysical application, 2. Relativistic shocks. *Astron. Astrophys. Rev.* **19**, 42 (2011). doi:10.1007/s00159-011-0042-8
- A. Bykov, N. Gehrels, H. Krawczynski, M. Lemoine, G. Pelletier, M. Pohl, Particle Acceleration in Relativistic Outflows. *Space Sci. Rev.* **173**, 309–339 (2012). doi:10.1007/s11214-012-9896-y
- N.F. Camus, S.S. Komissarov, N. Bucciantini, P.A. Hughes, Observations of ‘wisps’ in magnetohydrodynamic simulations of the Crab Nebula. *Mon. Not. R. Astron. Soc.* **400**, 1241–1246 (2009). doi:10.1111/j.1365-2966.2009.15550.x
- F. Casse, A. Marcowith, R. Keppens, Non-resonant magnetohydrodynamics streaming instability near magnetized relativistic shocks. *Mon. Not. R. Astron. Soc.* **433**, 940–951 (2013). doi:10.1093/mnras/stt772
- P. Chang, A. Spitkovsky, J. Arons, Long-Term Evolution of Magnetic Turbulence in Relativistic Collisionless Shocks: Electron-Positron Plasmas. *Astrophys. J.* **674**, 378–387 (2008). doi:10.1086/524764
- S.M. Couch, M. Milosavljević, E. Nakar, Shock Vorticity Generation from Accelerated Ion Streaming in the Precursor of Ultrarelativistic Gamma-Ray Burst External Shocks. *Astrophys. J.* **688**, 462–469 (2008). doi:10.1086/592194
- O.C. de Jager, A.K. Harding, The expected high-energy to ultra-high-energy gamma-ray spectrum of the Crab Nebula. *Astrophys. J.* **396**, 161–172 (1992). doi:10.1086/171706
- M. De Pasquale, Swift and Fermi Observations of the Early Afterglow of the Short Gamma-Ray Burst 090510. *Astrophys. J. Lett.* **709**, 146–151 (2010). doi:10.1088/2041-8205/709/2/L146
- L. Del Zanna, E. Amato, N. Bucciantini, Axially symmetric relativistic MHD simulations of Pulsar Wind Nebulae in Supernova Remnants. On the origin of torus and jet-like features. *Astron. Astrophys.* **421**, 1063–1073 (2004). doi:10.1051/0004-6361:20035936
- E.V. Derishev, Synchrotron emission in the fast cooling regime: which spectra can be explained? *Astrophys. Sp. Sc.* **309**, 157–161 (2007). doi:10.1007/s10509-007-9421-z
- E.V. Derishev, F.A. Aharonian, V.V. Kocharovsky, V.V. Kocharovsky, Particle acceleration through multiple conversions from a charged into a neutral state and back. *Phys. Rev. D* **68**(4), 043003 (2003). doi:10.1103/PhysRevD.68.043003
- D. Eichler, M. Pohl, Can Ultrahigh-energy Cosmic Rays Come from Gamma-Ray Bursts? Cosmic Rays Below the Ankle and Galactic Gamma-Ray Bursts. *Astrophys. J. Lett.* **738**, 21 (2011). doi:10.1088/2041-8205/738/2/L21
- D.C. Ellison, G.P. Double, Nonlinear particle acceleration in relativistic shocks. *Astroparticle Physics* **18**, 213–228 (2002). doi:10.1016/S0927-6505(02)00142-1
- D.C. Ellison, D.C. Warren, A.M. Bykov, Monte Carlo Simulations of Nonlinear Particle Acceleration in Parallel Trans-relativistic Shocks. *Astrophys. J.* **776**, 46 (2013). doi:10.1088/0004-637X/776/1/46

- G.D. Fleishman, Diffusive Synchrotron Radiation from Relativistic Shocks in Gamma-Ray Burst Sources. *Astrophys. J.* **638**, 348–353 (2006). doi:10.1086/498732
- J.T. Frederiksen, C.B. Hededal, T. Haugbølle, Å. Nordlund, Magnetic Field Generation in Collisionless Shocks: Pattern Growth and Transport. *Astrophys. J. Lett.* **608**, 13–16 (2004). doi:10.1086/421262
- D.L. Freedman, E. Waxman, On the Energy of Gamma-Ray Bursts. *Astrophys. J.* **547**, 922–928 (2001). doi:10.1086/318386
- Y.A. Gallant, M. Hoshino, A.B. Langdon, J. Arons, C.E. Max, Relativistic, perpendicular shocks in electron-positron plasmas. *Astrophys. J.* **391**, 73–101 (1992). doi:10.1086/171326
- M. Gedalin, M.A. Balikhin, D. Eichler, Efficient electron heating in relativistic shocks and gamma-ray-burst afterglow. *Phys. Rev. E* **77**(2), 026403 (2008). doi:10.1103/PhysRevE.77.026403
- M. Gedalin, E. Smolik, A. Spitkovsky, M. Balikhin, Electron heating by filamentary instability. *EPL (Europhysics Letters)* **97**, 35002 (2012). doi:10.1209/0295-5075/97/35002
- G. Ghisellini, G. Ghirlanda, L. Nava, A. Celotti, GeV emission from gamma-ray bursts: a radiative fireball? *Mon. Not. R. Astron. Soc.* **403**, 926–937 (2010). doi:10.1111/j.1365-2966.2009.16171.x
- A. Gruzinov, Gamma-Ray Burst Phenomenology, Shock Dynamo, and the First Magnetic Fields. *Astrophys. J. Lett.* **563**, 15–18 (2001). doi:10.1086/324223
- A. Gruzinov, E. Waxman, Gamma-Ray Burst Afterglow: Polarization and Analytic Light Curves. *Astrophys. J.* **511**, 852–861 (1999). doi:10.1086/306720
- T. Haugbølle, Three-dimensional Modeling of Relativistic Collisionless Ion-electron Shocks. *Astrophys. J. Lett.* **739**, 42 (2011). doi:10.1088/2041-8205/739/2/L42
- A.F. Heavens, L.O. Drury, Relativistic shocks and particle acceleration. *Mon. Not. R. Astron. Soc.* **235**, 997–1009 (1988)
- M. Hoshino, Wakefield Acceleration by Radiation Pressure in Relativistic Shock Waves. *Astrophys. J.* **672**, 940–956 (2008). doi:10.1086/523665
- M. Hoshino, J. Arons, Preferential positron heating and acceleration by synchrotron maser instabilities in relativistic positron-electron-proton plasmas. *Physics of Fluids B* **3**, 818–833 (1991). doi:10.1063/1.859877
- M. Hoshino, J. Arons, Y.A. Gallant, A.B. Langdon, Relativistic magnetosonic shock waves in synchrotron sources - Shock structure and nonthermal acceleration of positrons. *Astrophys. J.* **390**, 454–479 (1992). doi:10.1086/171296
- C.H. Jaroschek, H. Lesch, R.A. Treumann, Ultrarelativistic Plasma Shell Collisions in γ -Ray Burst Sources: Dimensional Effects on the Final Steady State Magnetic Field. *Astrophys. J.* **618**, 822–831 (2005). doi:10.1086/426066
- T.N. Kato, Relativistic Collisionless Shocks in Unmagnetized Electron-Positron Plasmas. *Astrophys. J.* **668**, 974–979 (2007). doi:10.1086/521297
- B. Katz, U. Keshet, E. Waxman, Self-Similar Collisionless Shocks. *ApJ* **655**, 375–390 (2007). doi:10.1086/509115
- S.R. Kelner, F.A. Aharonian, D. Khangulyan, On the Jitter Radiation. *Astrophys. J.* **774**, 61 (2013). doi:10.1088/0004-637X/774/1/61
- U. Keshet, Analytical Study of Diffusive Relativistic Shock Acceleration. *Physical Review Letters* **97**(22), 221104 (2006). doi:10.1103/PhysRevLett.97.221104
- U. Keshet, E. Waxman, Energy Spectrum of Particles Accelerated in Relativistic Collisionless Shocks. *Physical Review Letters* **94**(11), 111102 (2005). doi:10.1103/PhysRevLett.94.111102
- U. Keshet, B. Katz, A. Spitkovsky, E. Waxman, Magnetic Field Evolution in Relativistic Unmagnetized Collisionless Shocks. *Astrophys. J. Lett.* **693**, 127–130 (2009). doi:10.1088/0004-637X/693/2/L127
- J.G. Kirk, P. Duffy, TOPICAL REVIEW: Particle acceleration and relativistic shocks. *Journal of Physics G Nuclear Physics* **25**, 163 (1999). doi:10.1088/0954-3899/25/8/201
- J.G. Kirk, B. Reville, Radiative Signatures of Relativistic Shocks. *Astrophys. J. Lett.* **710**, 16–20 (2010). doi:10.1088/2041-8205/710/1/L16
- J.G. Kirk, P. Schneider, On the acceleration of charged particles at relativistic shock fronts. *Astrophys. J.* **315**, 425–433 (1987). doi:10.1086/165147
- J.G. Kirk, O. Skjæraasen, Dissipation in Poynting-Flux-dominated Flows: The σ -Problem

- of the Crab Pulsar Wind. *Astrophys. J.* **591**, 366–379 (2003). doi:10.1086/375215
- J.G. Kirk, A.W. Guthmann, Y.A. Gallant, A. Achterberg, Particle Acceleration at Ultrarelativistic Shocks: An Eigenfunction Method. *Astrophys. J.* **542**, 235–242 (2000). doi:10.1086/309533
- S.S. Komissarov, Y.E. Lyubarsky, Synchrotron nebulae created by anisotropic magnetized pulsar winds. *Mon. Not. R. Astron. Soc.* **349**, 779–792 (2004). doi:10.1111/j.1365-2966.2004.07597.x
- G.F. Krymskii, A regular mechanism for the acceleration of charged particles on the front of a shock wave. *Akademiia Nauk SSSR Doklady* **234**, 1306–1308 (1977)
- P. Kumar, R. Barniol Duran, On the generation of high-energy photons detected by the Fermi Satellite from gamma-ray bursts. *Mon. Not. R. Astron. Soc.* **400**, 75–79 (2009). doi:10.1111/j.1745-3933.2009.00766.x
- R. Kumar, D. Eichler, M. Gedalin, Electron Heating in a Relativistic, Weibel-Unstable Plasma. *ArXiv:astro-ph/1501.05466* (2015)
- A.B. Langdon, J. Arons, C.E. Max, Structure of relativistic magnetosonic shocks in electron-positron plasmas. *Physical Review Letters* **61**, 779–782 (1988). doi:10.1103/PhysRevLett.61.779
- M. Lemoine, Acceleration to ultra-high energies, in *American Institute of Physics Conference Series*, ed. by H. Sagawa, Y. Kawasaki, T. Sako, M. Takeda, Y. Tsunetsada American Institute of Physics Conference Series, vol. 1367, 2011, pp. 70–75. doi:10.1063/1.3628718
- M. Lemoine, Synchrotron signature of a relativistic blast wave with decaying microturbulence. *Mon. Not. R. Astron. Soc.* **428**, 845–866 (2013). doi:10.1093/mnras/sts081
- M. Lemoine, Nonlinear collisionless damping of Weibel turbulence in relativistic blast waves. *Journal of Plasma Physics* **81**, 45101 (2015). doi:10.1017/S0022377814000920
- M. Lemoine, G. Pelletier, Particle Transport in Tangled Magnetic Fields and Fermi Acceleration at Relativistic Shocks. *Astrophys. J. Lett.* **589**, 73–76 (2003). doi:10.1086/376353
- M. Lemoine, G. Pelletier, On electromagnetic instabilities at ultra-relativistic shock waves. *Mon. Not. R. Astron. Soc.* **402**, 321–334 (2010). doi:10.1111/j.1365-2966.2009.15869.x
- M. Lemoine, G. Pelletier, Dispersion and thermal effects on electromagnetic instabilities in the precursor of relativistic shocks. *Mon. Not. R. Astron. Soc.* **417**, 1148–1161 (2011). doi:10.1111/j.1365-2966.2011.19331.x
- M. Lemoine, B. Revenu, Relativistic Fermi acceleration with shock compressed turbulence. *Mon. Not. R. Astron. Soc.* **366**, 635–644 (2006). doi:10.1111/j.1365-2966.2005.09912.x
- M. Lemoine, E. Waxman, Anisotropy vs chemical composition at ultra-high energies. *J. Cosm. Astropart. Phys.* **11**, 9 (2009). doi:10.1088/1475-7516/2009/11/009
- M. Lemoine, K. Kotera, J. Pétri, On ultra-high energy cosmic ray acceleration at the termination shock of young pulsar winds. *ArXiv:astro-ph/1409.0159* (2014)
- M. Lemoine, Z. Li, X.-Y. Wang, On the magnetization of gamma-ray burst blast waves. *MNRAS* **435**, 3009–3016 (2013). doi:10.1093/mnras/stt1494
- M. Lemoine, G. Pelletier, B. Revenu, On the Efficiency of Fermi Acceleration at Relativistic Shocks. *ApJl* **645**, 129–132 (2006). doi:10.1086/506322
- M. Lemoine, G. Pelletier, L. Gremillet, I. Plotnikov, A fast current-driven instability in relativistic collisionless shocks. *EPL (Europhysics Letters)* **106**, 55001 (2014a). doi:10.1209/0295-5075/106/55001
- M. Lemoine, G. Pelletier, L. Gremillet, I. Plotnikov, Current-driven filamentation upstream of magnetized relativistic collisionless shocks. *Mon. Not. R. Astron. Soc.* **440**, 1365–1378 (2014b). doi:10.1093/mnras/stu213
- A. Levinson, Convective Instability of a Relativistic Ejecta Decelerated by a Surrounding Medium: An Origin of Magnetic Fields in Gamma-Ray Bursts? *ApJ Lett.* **705**, 213–216 (2009). doi:10.1088/0004-637X/705/2/L213
- Y. Lyubarsky, Electron-Ion Coupling Upstream of Relativistic Collisionless Shocks. *Astrophys. J.* **652**, 1297–1305 (2006). doi:10.1086/508606
- Y. Lyubarsky, D. Eichler, Are Gamma-Ray Burst Shocks Mediated by the Weibel Instability? *Astrophys. J.* **647**, 1250–1254 (2006). doi:10.1086/505523
- Y. Lyubarsky, J.G. Kirk, Reconnection in a Striped Pulsar Wind. *Astrophys. J.* **547**, 437–448 (2001). doi:10.1086/318354
- Y.E. Lyubarsky, The termination shock in a striped pulsar wind. *Mon. Not. R. Astron. Soc.*

- 345**, 153–160 (2003). doi:10.1046/j.1365-8711.2003.06927.x
- M.A. Malkov, L.O. Drury, Nonlinear theory of diffusive acceleration of particles by shock waves. *Reports on Progress in Physics* **64**, 429–481 (2001). doi:10.1088/0034-4885/64/4/201
- J. Mao, J. Wang, Gamma-ray Burst Prompt Emission: Jitter Radiation in Stochastic Magnetic Field Revisited. *Astrophys. J.* **731**, 26 (2011). doi:10.1088/0004-637X/731/1/26
- S.F. Martins, R.A. Fonseca, L.O. Silva, W.B. Mori, Ion Dynamics and Acceleration in Relativistic Shocks. *Astrophys. J. Lett.* **695**, 189–193 (2009). doi:10.1088/0004-637X/695/2/L189
- M.V. Medvedev, Theory of “Jitter” Radiation from Small-Scale Random Magnetic Fields and Prompt Emission from Gamma-Ray Burst Shocks. *Astrophys. J.* **540**, 704–714 (2000). doi:10.1086/309374
- M.V. Medvedev, The Theory of Spectral Evolution of the Gamma-Ray Burst Prompt Emission. *Astrophys. J.* **637**, 869–872 (2006). doi:10.1086/498697
- M.V. Medvedev, A. Loeb, Generation of Magnetic Fields in the Relativistic Shock of Gamma-Ray Burst Sources. *Astrophys. J.* **526**, 697–706 (1999). doi:10.1086/308038
- M.V. Medvedev, O.V. Zakutnyaya, Magnetic Fields and Cosmic Rays in GRBs: A Self-Similar Collisionless Foreshock. *Astrophys. J.* **696**, 2269–2274 (2009). doi:10.1088/0004-637X/696/2/2269
- M.V. Medvedev, M. Fiore, R.A. Fonseca, L.O. Silva, W.B. Mori, Long-Time Evolution of Magnetic Fields in Relativistic Gamma-Ray Burst Shocks. *Astrophys. J. Lett.* **618**, 75–78 (2005). doi:10.1086/427921
- M.V. Medvedev, J.T. Frederiksen, T. Haugbølle, Å. Nordlund, Radiation Signatures of Sub-Larmor Scale Magnetic Fields. *Astrophys. J.* **737**, 55 (2011). doi:10.1088/0004-637X/737/2/55
- A. Meli, J.J. Quenby, Particle acceleration in ultra-relativistic oblique shock waves. *Astroparticle Physics* **19**, 649–666 (2003). doi:10.1016/S0927-6505(02)00257-8
- M. Milosavljević, E. Nakar, The Cosmic-Ray Precursor of Relativistic Collisionless Shocks: A Missing Link in Gamma-Ray Burst Afterglows. *ApJ* **651**, 979–984 (2006a). doi:10.1086/507975
- M. Milosavljević, E. Nakar, Weibel Filament Decay and Thermalization in Collisionless Shocks and Gamma-Ray Burst Afterglows. *Astrophys. J.* **641**, 978–983 (2006b). doi:10.1086/500654
- S.S. Moiseev, R.Z. Sagdeev, Collisionless shock waves in a plasma in a weak magnetic field. *Journal of Nuclear Energy* **5**, 43–47 (1963). doi:10.1088/0368-3281/5/1/309
- E. Nakar, A. Bret, M. Milosavljević, Two-stream-like Instability in Dilute Hot Relativistic Beams and Astrophysical Relativistic Shocks. *Astrophys. J.* **738**, 93 (2011). doi:10.1088/0004-637X/738/1/93
- J. Niemiec, M. Ostrowski, Cosmic-Ray Acceleration at Relativistic Shock Waves with a “Realistic” Magnetic Field Structure. *Astrophys. J.* **610**, 851–867 (2004). doi:10.1086/421730
- J. Niemiec, M. Ostrowski, M. Pohl, Cosmic-Ray Acceleration at Ultrarelativistic Shock Waves: Effects of Downstream Short-Wave Turbulence. *ApJ* **650**, 1020–1027 (2006). doi:10.1086/506901
- M. Ostrowski, J. Bednarz, Comment on the first-order Fermi acceleration at ultra-relativistic shocks. *Astron. Astrophys.* **394**, 1141–1144 (2002). doi:10.1051/0004-6361:20021173
- G. Pelletier, M. Lemoine, A. Marcowith, Fermi Acceleration at Relativistic Shocks, in *American Institute of Physics Conference Series*, ed. by F.A. Aharonian, W. Hofmann, F. Rieger American Institute of Physics Conference Series, vol. 1085, 2008, pp. 61–70. doi:10.1063/1.3076750
- G. Pelletier, M. Lemoine, A. Marcowith, On Fermi acceleration and magnetohydrodynamic instabilities at ultra-relativistic magnetized shock waves. *MNRAS* **393**, 587–597 (2009). doi:10.1111/j.1365-2966.2008.14219.x
- I. Plotnikov, G. Pelletier, M. Lemoine, Particle transport and heating in the microturbulent precursor of relativistic shocks. *Mon. Not. R. Astron. Soc.* **430**, 1280–1293 (2013). doi:10.1093/mnras/sts696
- R.D. Preece, The Synchrotron Shock Model Confronts a “Line of Death” in the BATSE Gamma-Ray Burst Data. *Astrophys. J. Lett.* **506**, 23–26 (1998). doi:10.1086/311644

- I. Rabinak, B. Katz, E. Waxman, Long-wavelength Unstable Modes in the Far Upstream of Relativistic Collisionless Shocks. *ApJ* **736**, 157 (2011). doi:10.1088/0004-637X/736/2/157
- B. Reville, A.R. Bell, On the maximum energy of shock-accelerated cosmic rays at ultra-relativistic shocks. *Mon. Not. R. Astron. Soc.* **439**, 2050–2059 (2014). doi:10.1093/mnras/stu088
- B. Reville, J.G. Kirk, P. Duffy, A current-driven instability in parallel, relativistic shocks. *Plasma Physics and Controlled Fusion* **48**, 1741–1747 (2006). doi:10.1088/0741-3335/48/12/004
- E. Rossi, M.J. Rees, Gamma-ray burst afterglow emission with a decaying magnetic field. *Mon. Not. R. Astron. Soc.* **339**, 881–886 (2003). doi:10.1046/j.1365-8711.2003.06242.x
- R. Shaisultanov, Y. Lyubarsky, D. Eichler, Stream Instabilities in Relativistically Hot Plasma. *Astrophys. J.* **744**, 182 (2012). doi:10.1088/0004-637X/744/2/182
- L.O. Silva, R.A. Fonseca, J.W. Tonge, J.M. Dawson, W.B. Mori, M.V. Medvedev, Interpenetrating Plasma Shells: Near-equipartition Magnetic Field Generation and Nonthermal Particle Acceleration. *Astrophys. J. Lett.* **596**, 121–124 (2003). doi:10.1086/379156
- L. Sironi, J. Goodman, Production of Magnetic Energy by Macroscopic Turbulence in GRB Afterglows. *Astrophys. J.* **671**, 1858–1867 (2007). doi:10.1086/523636
- L. Sironi, A. Spitkovsky, Particle Acceleration in Relativistic Magnetized Collisionless Pair Shocks: Dependence of Shock Acceleration on Magnetic Obliquity. *Astrophys. J.* **698**, 1523–1549 (2009a). doi:10.1088/0004-637X/698/2/1523
- L. Sironi, A. Spitkovsky, Synthetic Spectra from Particle-In-Cell Simulations of Relativistic Collisionless Shocks. *Astrophys. J. Lett.* **707**, 92–96 (2009b). doi:10.1088/0004-637X/707/1/L92
- L. Sironi, A. Spitkovsky, Acceleration of Particles at the Termination Shock of a Relativistic Striped Wind. *Astrophys. J.* **741**, 39 (2011a). doi:10.1088/0004-637X/741/1/39
- L. Sironi, A. Spitkovsky, Particle Acceleration in Relativistic Magnetized Collisionless Electron-Ion Shocks. *Astrophys. J.* **726**, 75 (2011b). doi:10.1088/0004-637X/726/2/75
- L. Sironi, A. Spitkovsky, Particle-in-cell simulations of shock-driven reconnection in relativistic striped winds. *Computational Science and Discovery* **5**(1), 014014 (2012). doi:10.1088/1749-4699/5/1/014014
- L. Sironi, A. Spitkovsky, Relativistic Reconnection: An Efficient Source of Non-thermal Particles. *Astrophys. J. Lett.* **783**, 21 (2014). doi:10.1088/2041-8205/783/1/L21
- L. Sironi, M. Petropoulou, D. Giannios, Relativistic jets shine through shocks or magnetic reconnection? *Mon. Not. R. Astron. Soc.* **450**, 183–191 (2015). doi:10.1093/mnras/stv641
- L. Sironi, A. Spitkovsky, J. Arons, The Maximum Energy of Accelerated Particles in Relativistic Collisionless Shocks. *Astrophys. J.* **771**, 54 (2013). doi:10.1088/0004-637X/771/1/54
- A. Spitkovsky, Simulations of relativistic collisionless shocks: shock structure and particle acceleration, in *Astrophysical Sources of High Energy Particles and Radiation*, ed. by T. Bulik, B. Rudak, & G. Madejski AIP Conf. Ser., vol. 801, 2005, p. 345. doi:10.1063/1.2141897
- A. Spitkovsky, On the Structure of Relativistic Collisionless Shocks in Electron-Ion Plasmas. *Astrophys. J. Lett.* **673**, 39–42 (2008a). doi:10.1086/527374
- A. Spitkovsky, Particle Acceleration in Relativistic Collisionless Shocks: Fermi Process at Last? *Astrophys. J. Lett.* **682**, 5–8 (2008b). doi:10.1086/590248
- B.E. Stern, J. Poutanen, Radiation from relativistic jets in blazars and the efficient dissipation of their bulk energy via photon breeding. *Mon. Not. R. Astron. Soc.* **383**, 1695–1712 (2008). doi:10.1111/j.1365-2966.2007.12706.x
- A. Stockem, F. Fiúza, R.A. Fonseca, L.O. Silva, Acceleration in Perpendicular Relativistic Shocks for Plasmas Consisting of Leptons and Hadrons. *Astrophys. J.* **755**, 68 (2012). doi:10.1088/0004-637X/755/1/68
- P.-H.T. Tam, Q.-W. Tang, S.-J. Hou, R.-Y. Liu, X.-Y. Wang, Discovery of an Extra Hard Spectral Component in the High-energy Afterglow Emission of GRB 130427A. *Astrophys. J. Lett.* **771**, 13 (2013). doi:10.1088/2041-8205/771/1/L13
- X.-Y. Wang, R.-Y. Liu, M. Lemoine, On the Origin of >10 GeV Photons in Gamma-Ray Burst Afterglows. *Astrophys. J. Lett.* **771**, 33 (2013). doi:10.1088/2041-8205/771/2/L33
- E. Waxman, Gamma-Ray–Burst Afterglow: Supporting the Cosmological Fireball Model,

-
- Constraining Parameters, and Making Predictions. *Astrophys. J. Lett.* **485**, 5–8 (1997). doi:10.1086/310809
- J. Wiersma, A. Achterberg, Magnetic field generation in relativistic shocks. An early end of the exponential Weibel instability in electron-proton plasmas. *A&Ap* **428**, 365–371 (2004). doi:10.1051/0004-6361:20041882
- J. Zrake, Inverse Cascade of Nonhelical Magnetic Turbulence in a Relativistic Fluid. *Astrophys. J. Lett.* **794**, 26 (2014). doi:10.1088/2041-8205/794/2/L26